

The radio luminosity function from the low–frequency 3CRR, 6CE & 7CRS complete samples

Chris J. Willott^{1,2*}, Steve Rawlings¹, Katherine M. Blundell¹, Mark Lacy^{1,3,4} and Stephen A. Eales⁵

¹*Astrophysics, Department of Physics, Keble Road, Oxford, OX1 3RH, U.K.*

²*Instituto de Astrofísica de Canarias, C/ Via Lactea s/n, 38200 La Laguna, Tenerife, Spain*

³*Institute of Geophysics and Planetary Physics, L-413 Lawrence Livermore National Laboratory, Livermore, CA 94550, USA*

⁴*Department of Physics, University of California, 1 Shields Avenue, Davis CA 95616, USA*

⁵*Department of Physics and Astronomy, University of Wales Cardiff, P.O. Box 913, Cardiff CF2 3YB, U.K.*

26 April 2024

ABSTRACT

We measure the radio luminosity function (RLF) of steep-spectrum radio sources using three redshift surveys of flux-limited samples selected at low (151 & 178 MHz) radio frequency, low–frequency source counts and the local RLF. The redshift surveys used are the new 7C Redshift Survey (7CRS) and the brighter 3CRR and 6CE surveys totalling 356 sources with virtually complete redshift z information. This yields unprecedented coverage of the radio luminosity versus z plane for steep-spectrum sources, and hence the most accurate measurements of the steep-spectrum RLF yet made. We find that a simple dual-population model for the RLF fits the data well, requiring differential density evolution (with z) for the two populations. The low–luminosity population can be associated with radio galaxies with weak emission lines, and includes sources with both FRI and FRII radio structures; its comoving space density ρ rises by about one dex between $z \sim 0$ and $z \sim 1$ but cannot yet be meaningfully constrained at higher redshifts. The high–luminosity population can be associated with radio galaxies and quasars with strong emission lines, and consists almost exclusively of sources with FRII radio structure; its ρ rises by nearly three dex between $z \sim 0$ and $z \sim 2$. These results mirror the situation seen in X-ray and optically-selected samples of AGN where: (i) low luminosity objects exhibit a gradual rise in ρ with z which crudely matches the rises seen in the rates of global star formation and galaxy mergers; and (ii) the density of high luminosity objects rises much more dramatically. The integrated radio luminosity density of the combination of the two populations is controlled by the value of ρ at the low–luminosity end of the RLF of the high–luminosity population, a quantity which has been directly measured at $z \sim 1$ by the 7CRS. We argue that robust determination of this quantity at higher redshifts requires a new redshift survey based on a large (~ 1000 source) sample about five times fainter than the 7CRS.

Key words: radio continuum: galaxies – galaxies: active – quasars: general – galaxies: evolution

1 INTRODUCTION

The radio luminosity function (RLF) seeks to derive from observed samples and surveys of radio sources, their space density per unit co-moving volume and how this changes with source luminosity. It is an essential input to both grav-

itational lensing studies which probe cosmic geometry (e.g. Kochanek 1996) and modelling of the clustering of radio sources (Magliocchetti et al. 1998). The RLF derived at low radio frequencies is important for understanding the content of high frequency surveys and hence deriving jet beaming parameters (e.g. Jackson & Wall 1999). The shape and evolution of the RLF provide important constraints on the

*Email: cjw@astro.ox.ac.uk

nature of radio activity in massive galaxies and its cosmic evolution.

Longair (1966) was one of the first to attempt to determine the evolution of the radio source population. At that time there were very few radio source redshifts known and the main constraint upon his models came from the low-frequency source counts down to $S_{151} \approx 0.25$ Jy. Longair found that the data were best-fit by models where the most powerful radio sources undergo greater cosmic evolution (in comoving space density ρ) than less-powerful sources. The subsequent acquisition of a substantial fraction of the redshifts for the 3CRR complete sample of Laing, Riley & Longair (1983) enabled the evolution to be better constrained. Using the V/V_{\max} test (see Section 4) they concluded that the most powerful radio sources undergo substantial evolution with similar evolution for both powerful radio galaxies and quasars. Unfortunately, the tight correlation between radio luminosity and redshift in this sample meant that they were unable to make any progress on the form of the evolving RLF. Wall, Pearson & Longair (1980) suggested that complete samples a factor of ≈ 50 times fainter than the 3CRR sample would be necessary to differentiate between possible models of the RLF.

The most comprehensive study of the radio luminosity function prior to this work was performed by Dunlop & Peacock (1990; hereafter DP90). Using several complete samples selected at 2.7 GHz with lower flux-limits ranging from 2.0 Jy to 0.1 Jy, they considered the flat- and steep-spectrum populations separately and derived the RLF for each population. Their constraints on the RLF of flat-spectrum sources were somewhat tighter than those derived by Peacock (1985), but the major breakthrough of their paper concerned the constraints they were able to place on the RLF of steep-spectrum radio sources. The strong positive evolution in ρ with z out to $z \sim 2$ inferred by Longair (1966), Wall et al. (1980) and Laing et al. (1983) was mapped out in some detail, and more controversially their results indicated a decline in the co-moving number density of both populations beyond a redshift of ≈ 2 – the so-called ‘redshift cut-off’. DP90 concluded that for powerful sources a model of pure luminosity evolution (PLE – evolution only of the break luminosity with redshift, analogous to that of Boyle, Shanks & Peterson 1988 for the quasar optical luminosity function) fitted the data well (but only for $\Omega = 1$). A similar model which incorporates negative density evolution at high-redshift (the LDE model) was found to work well for both $\Omega = 1$ and $\Omega = 0$. A recent update on the DP90 work can be found in Dunlop (1998), and a critical re-evaluation of the evidence for a redshift cut-off in the flat-spectrum population can be found in Jarvis & Rawlings (2000).

Derivations of the luminosity functions of luminous AGN selected at all frequencies (radio, optical and X-ray) have shown a broken power-law form with a steeper slope at the high-luminosity end than at the low luminosity end (e.g. DP90, Boyle et al. 1988, Page et al. 1996). These studies were also able to adequately describe the positive evolution of the luminosity function from $z = 0$ to $z \approx 2$ by assuming pure luminosity evolution. More recent studies with different datasets have shown some deviations from PLE (e.g. Goldschmidt & Miller 1998, Miyaji, Hasinger & Schmidt 2000). The physical rationale behind PLE is that the AGN have long lifetimes (comparable with the Hubble Time) and they

decline in luminosity from $z \approx 2$ to $z = 0$. However, at least in the case of the high-luminosity radio population, we know such a model is not viable because the ages of FR II radio sources in the surveys are well-constrained to be \lesssim a few 10^8 yr (e.g. Blundell, Rawlings & Willott 1999). Furthermore, for X-ray and optically-selected quasars, accretion at the rates required for their high luminosities (over a Hubble Time) would lead to much more massive black holes than are observed in the local Universe (e.g. Cavaliere & Padovani 1989). Thus, although PLE models do fit the gross features of the data, the physical basis of these models is not clear.

The radio source population is composed of several seemingly different types of object. One division between types is concerned with radio structure which falls into two distinct classes: FRI, or ‘twin-jet’, sources; and FR II, or ‘classical double’, sources (Fanaroff & Riley 1974). At low luminosities $\log_{10}(L_{151}) \lesssim 25.5$, the vast majority of sources have an FRI radio structure (apart from the very low luminosity starbursts), whilst at higher luminosities the majority of sources have FR II structure. A second division is concerned with the optical properties of the population. At $\log_{10}(L_{151}) \sim 26.5$ the fraction of objects in low-frequency selected samples with observed broad-line nuclei changes rapidly from ≈ 0.4 at higher radio luminosities to ≈ 0.1 at lower luminosities (Willott et al. 2000). It is not yet clear whether this represents a fundamental change in central engine properties because, for example, it could be due to the opening angle of an obscuring torus increasing with decreasing luminosity (see Willott et al. 2000). However, it is clear that at least some FR II sources lack even indirect evidence for an active quasar nucleus because, as pointed out by Hine & Longair (1979) and Laing et al. (1994), they have weak or absent emission lines. Indeed it is plausible that the majority of FR II radio galaxies (per unit comoving volume) show passive elliptical-galaxy spectra (Rixon, Wall & Benn 1991) and are part of the low-luminosity population considered here.

In this paper we have chosen to investigate the RLF in terms of a dual-population model where the less radio-luminous population is composed of FR Is and FR IIs with weak/absent emission lines, and the more radio-luminous population of strong-line FR II radio galaxies and quasars. Our motivation for doing this is that the presence/absence of a quasar nucleus, as indicated by emission line strength, is a distinction intimately connected to the properties of the central engine, whereas radio structure is strongly influenced by the larger-scale environment (e.g. Kaiser & Alexander 1997). The critical radio luminosity [$\log_{10}(L_{151}) \sim 26.5$] which crudely divides the populations is also very close to the break in the RLF (e.g. from DP90), whereas the luminosity of the FRI/FR II divide is clearly well below the break. Tentative evidence for an increase in the fraction of quasars with redshift from $z = 0$ to $z \approx 1$ can then be explained if this low-luminosity population evolves less rapidly than the high-luminosity population (Willott et al. 2000). The ρ of FRI sources is already known to evolve less-strongly with z than that of the radio-luminous FR IIs (e.g. Urry & Padovani 1995), but here we will assume that this is because they are a sub-set of a larger population of low-luminosity radio sources, including FR IIs, which evolve less strongly. We will show that differential evolution between the two populations

mimics PLE to a certain extent, but with a more plausible physical basis.

Padovani & Urry (1992), Urry & Padovani (1995) and Jackson & Wall (1999) have adopted a different approach to determining the RLF from high-frequency complete samples. Instead of separating the flat- and steep-spectrum sources and deriving the RLF for each population, they use models built around unified schemes and relativistic beaming to determine the relative fractions of various classes of objects in the samples. Their models assume that BL Lac objects are the beamed versions of FRI and (in the case of Jackson & Wall) weak-line FRII radio galaxies, and that flat-spectrum quasars are favourably oriented FRII radio galaxies. However, both these analyses required the RLF of unbeamed objects to be determined independently, i.e. from low-frequency samples. Because they used only the 3CRR sample to determine the luminosity distribution of radio sources, the tight $L_{178} - z$ correlation meant a degeneracy between luminosity and redshift effects. Current models of this type are thus most useful for constraining the values of various beaming parameters and how these affect the population mix in high-frequency selected samples, and have not provided new information on the evolution of steep-spectrum sources.

In this paper we present a new investigation of the steep-spectrum RLF which combines the bright 3CRR sample with the new, fainter 6CE and 7CRS redshift surveys (based on the 6C and 7C radio surveys, respectively). Note that an investigation of the RLF of steep-spectrum quasars (based on the 3CRR and 7CRS samples) has been presented by Willott et al. 1998 (W98). As the basis for an investigation of the steep-spectrum RLF, the 3CRR/6CE/7CRS dataset improves on that used by DP90 in four different ways.

- **Spectroscopic completeness.** Many of the sources in the DP90 samples do not have spectroscopic redshifts [including, at the time of DP90, $\approx 50\%$ of the sources in their faintest sample – the Parkes Selected Regions (PSR)], and redshifts had to be estimated from the infrared Hubble diagram (the $K - z$ relation). Dunlop (1998) reports that further spectroscopy of these sources has shown their redshifts tended to be overestimated (due to the positive correlation between radio luminosity and K -band luminosity, Eales et al. 1997), which he contends strengthens the DP90 evidence for a redshift cut-off in high-frequency selected samples. However, as we discuss later (Section 5.1), the assignment of systematically high redshifts to many sources may in fact have caused DP90 to overestimate the strength of any redshift cut-off. In contrast to the PSR, the 6CE and 7CRS have virtually complete spectroscopic redshifts.

- **Coverage of the radio luminosity versus z plane.** The flux-limit of the PSR is $S_{2.7} = 0.1$ Jy. For steep-spectrum sources with $\alpha = 0.8$, this corresponds to $S_{151} \approx 1$ Jy, and for $\alpha = 1.2$ to $S_{151} \approx 3$ Jy, so the 7C Redshift Survey (7CRS) with a flux-limit of $S_{151} = 0.5$ Jy is a factor 2 – 6 times deeper at a given z than the PSR depending on spectral index. Because of the correlations between α and radio luminosity and z (e.g. Blundell et al. 1999) this makes the 7CRS sensitive to lower radio luminosity objects at the higher redshifts. Note that because the PSR covers an area

3.5 times larger than the 7CRS, the two samples actually contain similar numbers of high-redshift objects.

- **Radio completeness.** DP90 found the source counts in the PSR at 0.1 Jy to be a factor of two lower than expected from the source counts at other frequencies. They suggested that this is due to incompleteness in the original survey near its flux-limit, although this is by no means certain (J.V. Wall, priv. comm.). Although they attempted to correct for this, there remains some possibility of bias: methods based on the V/V_{\max} statistic are particularly sensitive to such problems, as objects close to the flux-limit have $V/V_{\max} \approx 1$, and losing such objects would bias the statistic towards a spuriously low value. The 6CE sample and the 7CRS are based on surveys which are complete at the flux-densities of interest. As Riley (1989) discusses, the number of large angular size sources omitted from surveys such as these due to surface brightness effects is likely to be negligible.

- **Benefits of low-frequency selection.** The ultimate goal of our programme is to model the evolution in the RLF of steep-spectrum sources. As detailed in Blundell et al. (1999), the physics of FRII radio sources means that the mapping between radio luminosity and one of the key physical variables, the bulk power in the jets, is much closer if the radio luminosity is evaluated at low rest-frame frequencies provided, of course, these lie above the synchrotron self-absorption frequency of a given source. Modelling of high frequency luminosity is much more problematic, both because lobe emission at these frequencies is highly sensitive to source age and redshift (because of inverse-Compton scattering of lobe electrons by the microwave background), and because Doppler-boosted cores and hotspots become much more important at high rest-frame frequencies.

In Section 2 we discuss the data available to constrain the steep-spectrum RLF. Section 3 describes the model fitting procedures and results. In Section 4 the evolution of the radio source population is tested via the V/V_{\max} statistic. Section 5 compares our findings with those of previous RLF determinations. In Section 6 we summarise our results and indicate the future work necessary to resolve the outstanding uncertainties.

The convention for the radio spectral index, α_{rad} , is that $S_{\nu} \propto \nu^{-\alpha_{\text{rad}}}$, where S_{ν} is the flux-density at frequency ν . We assume throughout that $H_0 = 50 \text{ km s}^{-1} \text{ Mpc}^{-1}$ and $\Omega_{\Lambda} = 0$. All results are presented for both flat ($\Omega_{\text{M}} = 1$) and open ($\Omega_{\text{M}} = 0$) cosmologies.

2 CONSTRAINING DATA

The radio luminosity function (RLF) is defined as the number of radio sources per unit co-moving volume per unit (base 10) logarithm of luminosity, $\rho(L, z)$. To determine the RLF, we will make use of three different types of radio data: complete samples with spectroscopic redshifts; source counts; and a low-redshift sample to fix the local RLF.

2.1 Complete samples

A complete sample consists of every radio source in a certain area on the sky brighter than a specified flux-limit at

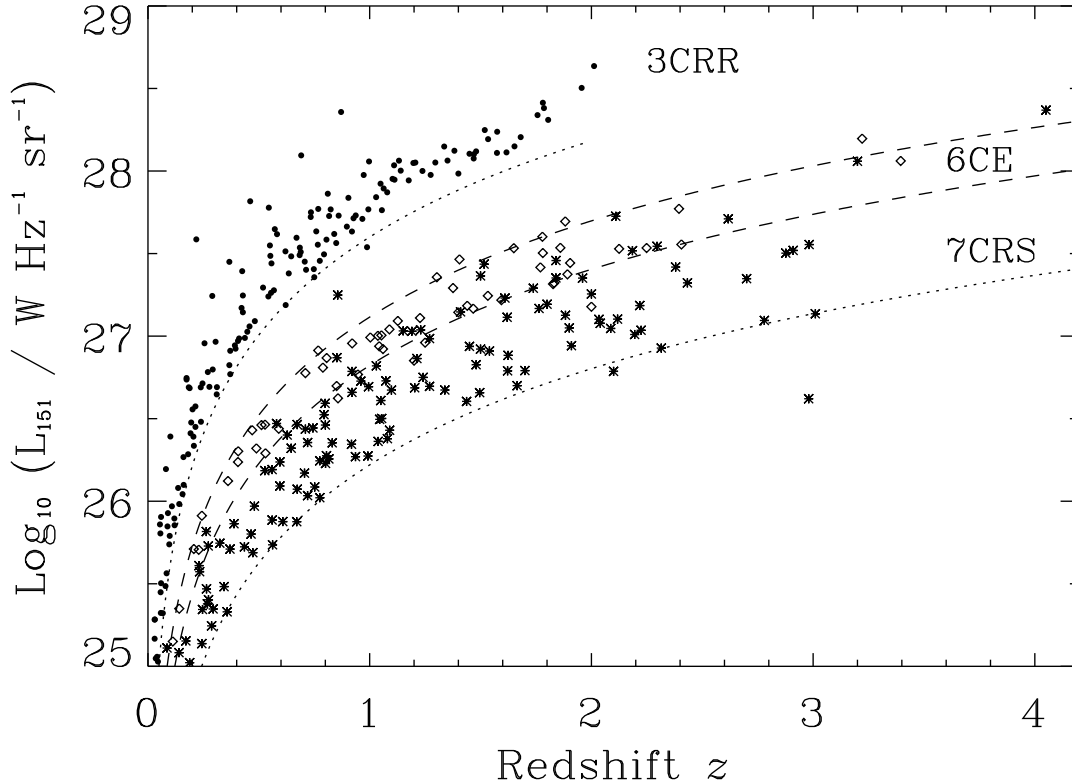


Figure 1. The radio luminosity–redshift plane for the 3CRR, 6CE and 7CRS samples described in Section 2.1. The different symbols identify sources from different samples: 3CRR (filled circles), 6CE (open diamonds) and 7CRS (asterisks). The dotted lines show the flux-density lower limits for the 3CRR and 7CRS samples and the dashed lines the limits for the 6CE sample (all assuming a radio spectral index of 0.5). This plot is for $\Omega_M = 1$, $\Omega_\Lambda = 0$.

the selection frequency. If all these sources are identified optically with a galaxy or quasar and redshifts are determined, then the distribution of points on the $L - z$ plane, together with knowledge of the sample flux-limits and sky areas, in principle allow the determination of the RLF. The major uncertainty in such a determination is that at least some regions of the $L - z$ plane will be very sparsely populated, and at these L and z the RLF measurement will be prone to small number statistical uncertainties. These typically arise because the identification of and/or redshift acquisition of faint radio sources can be very time-consuming, and due to the limited nature of time available at large telescopes, complete samples up until now have generally been limited to $\lesssim 100$ sources. Some regions of the $L - z$ plane are prone to a more fundamental problem: objects of a given L may be sufficiently rare that there is simply too little observable comoving volume at the redshift of interest to obtain large samples.

Our dataset of redshift surveys combines three low-frequency complete samples with different flux-limits, which together provide unparalleled coverage of the $L_{151} - z$ plane (see Fig. 1).

2.1.1 7CRS

The faintest of the three complete samples used is the new 7C Redshift Survey (7CRS). This sample contains every source with a low-frequency flux-density $S_{151} \geq 0.5$ Jy in three regions of sky covering a total of 0.022 sr. The regions 7C-I and 7C-II will be described in Blundell et al. (in prep.) and 7C-III in Lacy et al. (1999a) and references therein. For 7C-I and 7C-II, multi-frequency radio data including high-resolution radio maps from the VLA will be presented in Blundell et al. From measurements at several frequencies, the radio spectra have been fitted and hence radio luminosities at rest-frame 151 MHz determined. Spectral indices at various frequencies were also determined from these fits. For 7C-III, the availability of 38 MHz data from the 8C survey in the same region has allowed the low-frequency spectral indices to be calculated and hence rest-frame 151 MHz luminosities (Lacy et al. 1999a).

Due to the low-frequency selection of the sample, it is expected to contain few flat-spectrum ($\alpha_{1\text{GHz}} < 0.5$) sources. From inspection of the VLA maps and radio spectra, sources which only have flux-densities above the sample limit due to their Doppler-boosted cores can be identified. Out of the total of 130 sources, only one source fulfills these criteria – the quasar 5C7.230. Therefore this source is excluded from the analysis presented in this paper.

Note however that there are five other quasars which have $\alpha_{1\text{GHz}} < 0.5$, the traditional separation value between flat- and steep-spectrum quasars. All of these have $\alpha_{1\text{GHz}} \approx 0.4$ and are compact ($\theta < 5$ arcsec), but have extended emission on *both* sides of the core, indicating that Doppler-boosting is not the cause of this emission. They all have sufficient extended flux to remain in the sample and as such they are not excluded on orientation bias grounds. These sources are referred to as Core-JetS sources (CJSs; see Blundell et al. in prep. for more details). The one other exclusion is 3C200, because it is already included in the 3CRR sample, leaving a total of 128 sources.

All 7C Redshift Survey sources have been reliably identified with an optical/near-infrared counterpart. For 7C-I and 7C-II, spectroscopy has been attempted on all sources and secure redshifts obtained for $> 90\%$ of the sample (Willott et al., in prep.). Seven sources do not show any emission or absorption lines in their spectra. For these objects, we have obtained multi-colour optical and near-infrared photometry (in the R , I , J , H and K bands) to attempt to constrain their redshifts. All of these objects have spectral energy distributions consistent with evolved stellar populations at redshifts in the range $1 \leq z \leq 2$ (Willott, Rawlings & Blundell 2000). These derived redshifts are generally consistent with those from the $K - z$ diagram, particularly given the increased scatter in the relationship at faint magnitudes (Eales et al. 1997). Note that radio galaxies in the redshift range $1.3 < z < 1.8$ are traditionally difficult to obtain redshifts for because there are no bright emission lines in the optical wavelength region. The correlation between emission line and radio luminosities (Baum & Heckman 1989; Rawlings & Saunders 1991; Willott et al. 1999) exacerbates this problem for faint radio samples. We believe that this is the primary reason why we have been unable to detect emission lines in these 7 sources. It is extremely unlikely that any of these objects actually lie at $z > 2.5$.

Details of the imaging and spectroscopy in the 7C-III region are given in Lacy et al. (1999a, 1999b, 2000). Reasonably secure spectroscopic redshifts have been obtained for 81% of the sources and uncertain redshifts for a further 13%. Near-infrared magnitudes recently obtained support these uncertain redshifts. Only three sources have no redshift information. Near-infrared and optical imaging shows that two of them have SEDs typical of $z \approx 1.5$ galaxies as is the case for those without spectroscopic redshifts in 7C-I and 7C-II. The other object (7C1748+6703) has a break between J and K that is suggestive of a redshift $z > 2.4$. The existence of significant flux in its optical spectrum down to 6000 Å and a K -magnitude of 18.9, suggest $z < 4$. Therefore we adopt $z = 3.2$ in this paper.

2.1.2 3CRR

The bright complete sample used is the 3CRR sample of Laing, Riley & Longair (1983, hereafter LRL) with complete redshift information for all 173 radio sources. The flux-limit is 10.9 Jy at 178 MHz, which translates to 12.4 Jy at 151 MHz assuming a typical spectral index of 0.8. Blundell et al. (in prep.) review the current status of this sample and presents the results of spectral fitting of multi-frequency radio data. 3C231 (M82) is excluded because the radio emission from this source is due to a starburst and not an AGN.

The two flat-spectrum quasars, 3C345 and 3C454.3, are excluded because only Doppler-boosting of their core fluxes raises their total fluxes above the flux-limit. To include objects such as these would cause an overestimate in the number density of AGN, since they only get into the samples because their jet axes are very close to our line-of-sight. Note that high-frequency selected samples contain a much higher proportion of objects such as these, showing that our choice of low-frequency selection virtually eliminates these favourably oriented sources [there are only three such sources ($\approx 1\%$) in our complete samples].

2.1.3 6CE

The 6CE complete sample we use is a revision of the 6C sample of Eales (1985) (see Rawlings, Eales & Lacy 2000 for details). The flux-limits of this sample are $2.0 \leq S_{151} < 3.93$ Jy and the sky area covered is 0.103 sr. Only 3 of the 59 sources in this sample do not have redshifts determined from spectroscopy. One object is occluded by a bright star and is excluded from further consideration (without bias). One object is faint in the near-infrared ($K > 19$), so we take it as a galaxy at $z = 2.0$ in this paper. The other is relatively bright in the near-IR but very faint in the optical. Its red colour suggests a galaxy with a redshift in the range $0.8 < z < 2$ and we assume $z = 1.4$ here. None of the 6CE sources are clearly promoted into the sample by Doppler-boosted core emission (c.f. 5C7.230, 3C345 and 3C454.3), so all 58 sources are included in our analysis. Full details of the sample, including optical spectra, are given in Rawlings et al. (2000).

2.2 The source counts at 151 MHz

The three complete samples with known redshift distributions contain a total of 356 sources (after the exclusions mentioned above). However, the number of radio sources at 151 MHz as a function of flux density, also known as the source counts, has been determined for thousands of sources from the much larger sky area 6C and 7C surveys (Hales, Baldwin & Warner 1988 and McGilchrist et al. 1990, respectively). The 7C source counts go as faint as 0.1 Jy – a factor of five fainter than the 7CRS. At these flux-densities the source counts are our only constraint on the RLF. At the bright end ($\gtrsim 10$ Jy), the source counts are obtained by binning the sources in the 3CRR sample of LRL in 5 flux bins. The three sources excluded in Section 2.1 were also excluded for the calculation of the source counts. The 3CRR source counts are converted from 178 to 151 MHz by assuming a spectral index of 0.8.

Figure 2 shows the binned differential source counts from the 3CRR, 6C and 7C surveys. The counts are normalised to the differential source counts for a uniform distribution in a Euclidean universe, such that $dN_0 = 2400 (S_{\min}^{-1.5} - S_{\max}^{-1.5})$, where S_{\min} and S_{\max} are the lower and upper flux limits of the bin. These points were fitted by a third-order polynomial using a least-squares fit in logarithm space, i.e.

$$\log_{10} \left(\frac{dN}{dN_0} \right) = \frac{a_0 + a_1 \log_{10} S_{151} + a_2 (\log_{10} S_{151})^2 + a_3 (\log_{10} S_{151})^3}{a_2 (\log_{10} S_{151})^2 + a_3 (\log_{10} S_{151})^3}. \quad (1)$$

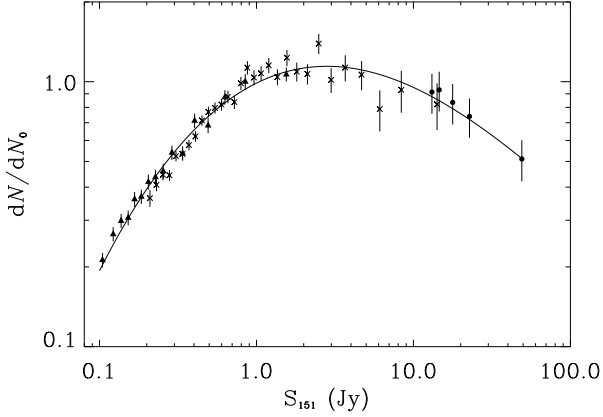


Figure 2. The binned differential source counts from the 3CRR (LRL), 6C (Hales et al. 1988) and 7C (McGilchrist et al. 1990) surveys. Error bars are \sqrt{N} Poisson errors for the number of sources in each bin. The symbols identify the surveys: 3CRR (circles), 6C (crosses) and 7C (triangles). The line shows the third-order polynomial fit to the data points.

The coefficients of the fit are $a_0 = -0.00541$, $a_1 = 0.293$, $a_2 = -0.362$ and $a_3 = 0.0527$. A higher order polynomial was not required to provide a decent fit to the data. The error on this curve was estimated using the errors from the source count bins. At $S_{151} \leq 1.0$ Jy the fractional errors on the bins are approximately constant with flux-density at the level of 0.06. At $S_{151} > 1.0$ Jy the fractional errors are given by a power-law with slope 0.49 such that the fractional error at 10 Jy is 0.19, for example.

It is well known that there is a flattening of the source counts slope at 1.4-GHz flux-densities ~ 1 mJy. This is attributed to the counts becoming dominated by low-redshift star-forming galaxies (Condon 1984; Windhorst et al. 1985). Although there is only one such starburst galaxy in our complete samples down to 0.5 Jy (3C231), the source count data goes as low as 0.1 Jy, so it is essential to investigate the contribution of starburst galaxies to the source counts at these low flux-densities. To estimate the starburst contribution we used the $60\mu\text{m}$ luminosity function of Saunders et al. (1990) scaled by the mean of the ratio of IRAS $60\mu\text{m}$ to NVSS 1.4 GHz flux-densities (Cotton & Condon 1998). Cosmic evolution is accounted for by the PLE model adopted by Saunders et al. To translate this 1.4 GHz luminosity function to 151 MHz, a spectral index of 0.7 was assumed for the starburst population. The differential source counts at 151 MHz were then calculated from this luminosity function. It is found that the starburst contribution at 0.1 Jy is only 2% of the total source counts. This is within the uncertainty in the source counts at 0.1 Jy, so it can be safely neglected.

2.3 The local RLF

The radio luminosity function at low-redshift ($z \lesssim 0.2$) is fairly well-determined. This therefore provides a boundary condition for determination of the evolving RLF. Unfortunately, the low space density of powerful radio sources and small cosmological volume out to $z \approx 0.2$ means that the local RLF (LRLF) is only well-constrained at radio luminosities

below $L_{151} \approx 10^{24} \text{ W Hz}^{-1} \text{ sr}^{-1}$. Hence the LRLF will only constrain the faint end of the RLF. Another problem is that at very low luminosities ($L_{151} \approx 10^{21} \text{ W Hz}^{-1} \text{ sr}^{-1}$) the LRLF is dominated by the star-forming spiral/irregular galaxies which dominate the sub-mJy (at 1.4 GHz) source counts. Since we do not want to include this population in our RLF determination, it is essential that the LRLF of the AGN population only is used.

A determination of the local radio luminosity function which treats AGN and star-forming galaxies as two distinct populations is given by Cotton & Condon (1998). By cross-matching UGC galaxies (Nilson 1973) with the NVSS catalogue (Condon et al. 1998) they derived luminosity functions at 1.4 GHz for each population. The AGN LRLF at 151 MHz was derived from this by assuming a radio spectral index of 0.8. This determination of the LRLF by Cotton & Condon is well-approximated by a power-law (up to $L_{151} \approx 10^{24} \text{ W Hz}^{-1} \text{ sr}^{-1}$) with an index of -0.53 . From this model the LRLF was determined in 10 bins in the range $20 \leq \log_{10}(L_{151}/\text{W Hz}^{-1} \text{ sr}^{-1}) \leq 23.6$. The error on each bin was assumed to be 0.1 dex.

3 MODEL FITTING

3.1 Method

To find best-fit parameters for various models of the evolving RLF, a maximum likelihood method is adopted. This method is similar to that used in W98 to determine the quasar RLF and we refer readers to that paper for further details. The aim of the maximum likelihood method is to minimise the value of S , which is defined as

$$S = -2 \sum_{i=1}^N \ln[\rho(L_i, z_i)] + 2 \iint \rho(L, z) \Omega(L, z) \frac{dV}{dz} dz d \log_{10} L, \quad (2)$$

where $(dV/dz)dz$ is the differential co-moving volume element, $\Omega(L, z)$ is the sky area available from the samples for these values of L and z and $\rho(L, z)$ is the model distribution being tested. In the first term of this equation, the sum is over all the N sources in the combined sample. The second term is simply the integrand of the model being tested and should give $\approx 2N$ for good fits.

The only difference here is that the source counts and local radio luminosity function provide additional constraints for the fitting process. The source counts and LRLF are one-dimensional functions and to estimate how well they fit the model, the value of χ^2 is evaluated thus:

$$\chi^2 = \sum_{i=1}^N \left(\frac{f_{\text{data } i} - f_{\text{mod } i}}{\sigma_{\text{data } i}} \right)^2, \quad (3)$$

where $f_{\text{data } i}$ is the value of the data in the i th bin, similarly $f_{\text{mod } i}$ and $\sigma_{\text{data } i}$ are the model value and data error in the i th bin, respectively. These are all determined in logarithm space for both the source counts and the LRLF. The sum is over the N bins in each case.

In order to combine the constraints from all three types of data, we follow Kochanek (1996). χ^2 is related to the

likelihood by $\chi^2 = -2 \ln(\text{likelihood})$, i.e. the same form as S . Therefore the function that is now minimised is

$$S_{\text{all}} = \chi_{\text{SC}}^2 + \chi_{\text{LRLF}}^2 + S - S_0, \quad (4)$$

where S_0 is a constant which normalises S so that equal statistical weight is given to all three types of data. The value of S_0 theoretically comes from the dropped terms from equation 2. However, these are not possible to calculate directly, so instead one estimates the value of S_0 so that the first term in equation 2 equals ≈ 0 and $S \approx 2N$. Errors on the best-fit parameters are 68% confidence levels, as discussed in Boyle et al. (1988).

The goodness-of-fit of models are estimated using the 2-D Kolmogorov-Smirnov (KS) test (Peacock 1983), as in W98. Note that it is expected that the KS probabilities will be lower than for the quasar RLF fits, because in general the probability decreases with increased sample size in this test. Simulations of the $L_{151} - z$ plane are used to double check the goodness-of-fit. In addition, the predicted redshift distributions for the complete samples are derived from the models and compared with the actual distribution. This is particularly useful in testing for the presence of a redshift cut-off at high- z .

3.2 The form of the RLF

As explained in Sec. 1, the RLF is modelled here as a combination of two populations which are allowed to have different RLF shapes and evolutionary properties. The low-luminosity radio source population (composed of FRIs and low-excitation/weak emission line FRIIs) is modelled with a Schechter function,

$$\rho_1(L) = \rho_{1\circ} \left(\frac{L}{L_{1\star}} \right)^{-\alpha_1} \exp \left(\frac{-L}{L_{1\star}} \right), \quad (5)$$

where $\rho_1(L)$ is the source number density as a function of radio luminosity L , $\rho_{1\circ}$ is a normalisation term, $L_{1\star}$ is the break luminosity and α_1 is the power-law slope. The evolution function of ρ_1 is modelled as $f_1(z) = (1+z)^{k_1}$ up to a maximum redshift $z_{1\circ}$ beyond which there is no further evolution. Hence there are five free parameters to be fixed for the low-luminosity population.

For the high-luminosity population a similar form is adopted, except in this case the exponential part of the Schechter function is at low luminosity and the power-law region is at high luminosity, i.e.

$$\rho_h(L) = \rho_{h\circ} \left(\frac{L}{L_{h\star}} \right)^{-\alpha_h} \exp \left(\frac{-L_{h\star}}{L} \right), \quad (6)$$

where the subscript h refers to the high luminosity population. Note that it is expected that $L_{1\star} \approx L_{h\star}$, so that at this luminosity the decline in one population is compensated by the rise of the other, since no discontinuity or bimodality in the RLF has yet been observed (e.g. DP90). These forms for the luminosity functions of the two populations were chosen because the steep exponentials ensured a fairly small overlap in L_{151} between the two populations. However, we currently have little information about the relative population fractions in the overlap region, so this is just a convenient method of separating the populations. We note that the low-luminosity RLF of our model has a sim-

ilar shape to the elliptical galaxy K -band luminosity (and therefore mass) function (e.g. Gardner et al. 1997).

The high-luminosity population is assumed to undergo density evolution of a similar form to that of the quasar RLF in W98. The z -distribution $f_h(z)$ is given by a Gaussian in redshift (model A here), with a variant on this distribution being a one-tailed Gaussian from zero redshift to the peak redshift and then a constant density to high-redshift (model B – also known as the ‘no cut-off’ model since there is no redshift cut-off). Note that the Gaussian model A is a convenient approximation to the shape of the evolution of luminous optically-selected quasars (e.g. Warren, Hewett & Osmer 1994), and to the evolution inferred for flat-spectrum radio sources by Shaver et al. (1999) – but see Jarvis & Rawlings (2000) for a contrary view. There is no physical reason why one would expect the evolution to be symmetric in redshift. In W98 we showed that the Gaussian redshift distribution from $z = 0$ to the peak is very similar to the form $(1+z)^k$, so we do not include models with this form of evolution here.

In W98 it was found that both these redshift distributions (models A and B in this paper) provided good fits because the number of quasars in the samples at high-redshift was fairly small. The inclusion of the 6CE and 7C-III samples and the 7CRS radio galaxies gives a much larger sample of $z > 2$ objects here than for the quasar RLF. Hence, the high redshift evolution can be better determined. Therefore, an additional redshift distribution is tested here, which has a one-tailed Gaussian rise to the peak redshift and then a one-tailed Gaussian decline at higher redshifts which is allowed to have a different width from the rise. This allows more shallow high-redshift declines in ρ_h (such as that inferred by DP90) than the symmetric model A. This model (C) directly fits the strength of any decline in the co-moving density beyond the peak redshift $z_{h\circ}$, since the value of the high-redshift Gaussian width z_{h2} is free to be fit from 0 for an abrupt cut-off to a large value for a very gradual decline at high-redshift. Hence there are a total of six free parameters in the high-luminosity population model with this form of redshift evolution.

To summarise our adopted RLF models, below we give all the equations needed to reproduce the RLF $\rho(L, z)$. The values of the best-fit parameters are given in Table 1.

$$\rho(L, z) = \rho_1 + \rho_h \quad (7)$$

where

$$\rho_1 = \rho_{1\circ} \left(\frac{L}{L_{1\star}} \right)^{-\alpha_1} \exp \left(\frac{-L}{L_{1\star}} \right) (1+z)^{k_1} \quad \text{for } z < z_{1\circ}, \quad (8)$$

$$\rho_1 = \rho_{1\circ} \left(\frac{L}{L_{1\star}} \right)^{-\alpha_1} \exp \left(\frac{-L}{L_{1\star}} \right) (1+z_{1\circ})^{k_1} \quad \text{for } z \geq z_{1\circ}, \quad (9)$$

$$\rho_h = \rho_{h\circ} \left(\frac{L}{L_{h\star}} \right)^{-\alpha_h} \exp \left(\frac{-L_{h\star}}{L} \right) f_h(z). \quad (10)$$

The high-luminosity evolution function $f_h(z)$ has three different forms depending upon the model and the redshift:

$$f_h(z) = \exp \left\{ -\frac{1}{2} \left(\frac{z - z_{h\circ}}{z_{h1}} \right)^2 \right\} \quad (11)$$

for model A at all redshifts and models B and C at $z < z_{h\circ}$;

$$f_h(z) = 1.0 \quad (12)$$

for model B at $z \geq z_{\text{ho}}$;

$$f_{\text{h}}(z) = \exp \left\{ -\frac{1}{2} \left(\frac{z - z_{\text{ho}}}{z_{\text{h2}}} \right)^2 \right\} \quad (13)$$

for model C at $z \geq z_{\text{ho}}$.

In this paper, we have performed the RLF modelling for two cosmological models with $\Omega_{\text{M}} = 1$ and $\Omega_{\text{M}} = 0$ and zero cosmological constant. To obtain a fairly reliable estimate of the RLF in other cosmologies one can use the following relation from Peacock (1985),

$$\rho_1(L_1, z) \frac{dV_1}{dz} = \rho_2(L_2, z) \frac{dV_2}{dz}, \quad (14)$$

where L_1 and L_2 are the luminosities derived from the flux-density and redshift in the two cosmologies. We have tested this relation by converting our model C RLF derived for $\Omega_{\text{M}} = 0$ back to $\Omega_{\text{M}} = 1$ and then compared this with the RLF derived for $\Omega_{\text{M}} = 1$. We note that the relation works well for regions of the luminosity function that are well-constrained by data. However, in regions which are constrained by little or no data, the relation may not reproduce a model RLF close to that which would emerge from direct fitting to the data in the new cosmology. Thus, Table 1 shows that the model C peak redshifts z_{ho} and strength of high- z decline z_{h2} are different for $\Omega_{\text{M}} = 1$ and $\Omega_{\text{M}} = 0$ and equation 14 cannot reproduce such differences. Note that the RLF for $\Omega_{\text{M}} = 0.3$, $\Omega_{\Lambda} = 0.7$ is very similar to that of $\Omega_{\text{M}} = 0$, $\Omega_{\Lambda} = 0$ for regions of the RLF well-constrained by our data and equation 14 can be applied in this case.

3.3 Results

The maximum likelihood fitting routine was run for these three RLF models. The routine integrated over the ranges $20 < \log_{10}(L_{151}) < 30$ and $0 < z < 5$. A check was made to ensure that the same results occurred if the redshift range was increased to $z = 10$. All three models provided good fits to the data. The best-fit parameters for each model are shown in Table 1.

The parameters for the low-luminosity population RLF do not change significantly for the different models, which is as expected, since it has little to do with the form of the high- z evolution of the high-luminosity RLF. Note that the value of the break luminosity, $\log(L_{1\star}) \approx 26.1$ (26.5 for $\Omega_{\text{M}} = 0$), is above the FRI/FRII divide and below the break in the quasar RLF from W98 [$\log(L_{\text{break}}) \approx 26.8$ (27.2 for $\Omega_{\text{M}} = 0$)]. The models show significant evolution ($k_1 \approx 4$) for the low-luminosity objects out to $z \approx 0.7$ with no further evolution to higher redshifts. Although it is often stated that the FRI radio galaxy population shows no evolution, the samples used to determine this generally have small numbers of objects and a narrow redshift range (e.g. Urry, Padovani & Stickel 1991; Jackson & Wall 1999). As we shall see in Section 4 the combination of the 3CRR, 6CE and 7CRS samples shows considerable low-redshift evolution for low-luminosity ($\log_{10} L_{151} \lesssim 26.5$) FRI and FRII radio galaxies.

The best-fit models for the high-luminosity RLF have much steeper slopes than the low-luminosity RLF ($\alpha_{\text{h}} \approx 2.3$, c.f. $\alpha_1 \approx 0.6$). This, together with $\log(L_{1\star}) \sim \log(L_{\text{h}\star})$, gives the whole RLF a broken power-law form, such as observed by DP90 for the RLF and by Boyle et al. (1988) for the

Model	Ω_{M}	N_{par}	P_{KS}
A	1	10	0.11
B	1	10	0.28
C	1	11	0.36
A	0	10	0.03
B	0	10	0.09
C	0	11	0.07

Table 2. Goodness-of-fit table. N_{par} is the number of free parameters in the model (including those from both the low- and high-luminosity populations) and P_{KS} is the probability from the 2D K-S test to the $L_{151} - z$ distribution. As in Table 1 the top three rows refer to $\Omega_{\text{M}} = 1$ and the bottom three to $\Omega_{\text{M}} = 0$.

quasar OLF. $L_{\text{h}\star}$ in these models is about an order of magnitude greater than $L_{1\star}$ and is very similar to the break in the quasar RLF estimated in W98 from source counts constraints. The RLF of model C at various redshifts is shown in Figure 3. The broken power-law form for the whole population can clearly be seen at $z \lesssim 1$. At higher redshifts the continued evolution of the high-luminosity population causes the RLF to have a small dip at $\log(L_{151}) \approx 26.2$ (26.6 for $\Omega_{\text{M}} = 0$). This is a consequence of the models chosen and may or may not be real. No previous low-frequency complete samples have gone to such low flux-density levels to constrain this region of the $L_{151} - z$ plane directly. In fact, for $\log(L_{151}) \approx 26.2$ and $z > 1$, the 151 MHz flux-density of any sources would be fainter than the limit of the 7CRS sample and the RLF is purely constrained by the source counts in this region. The maximum size of this feature is only 0.2 dex, so it would be extremely difficult to confirm directly by measurement of the RLF.

Fig. 4 shows the calculated source counts at 151 MHz from the model C RLFs for $\Omega_{\text{M}} = 1$ and $\Omega_{\text{M}} = 0$. The counts from each of the two parts of the RLF have also been plotted separately. The models fit the total source counts very well, as is expected because the maximum likelihood method minimises the χ^2 of the fit to the source counts data. For both cosmologies, the high-luminosity population dominates the source counts over most of the flux-density range. The low-luminosity population starts to dominate at ~ 0.2 Jy. This suggests that fainter samples, such as those selected at flux-limits $S_{151} \geq 0.1$ Jy, would contain more low-luminosity population sources. This idea will be discussed further in Section 6.

We now briefly consider whether it is obvious that any of these three models provides the best-fit to the data and hence whether we can usefully constrain the strength of any high- z decline in the co-moving space density ρ of radio sources. We defer a full statistical analysis of this question to a future paper (Jarvis et al., 2000) in which data from the 3CRR and 6CE complete samples is combined with the results of targeted searches for $z > 4$ radio galaxies (the 6C* sample of Blundell et al. 1998). Figure 5 shows the redshift-dependence of the high-luminosity RLF for these three models with their free parameters fixed at the best-fit values. All the models provide good fits to both the source counts and local RLF data, with reduced χ^2 values of order one. Table 2 shows the goodness-of-fit (KS test probabilities)

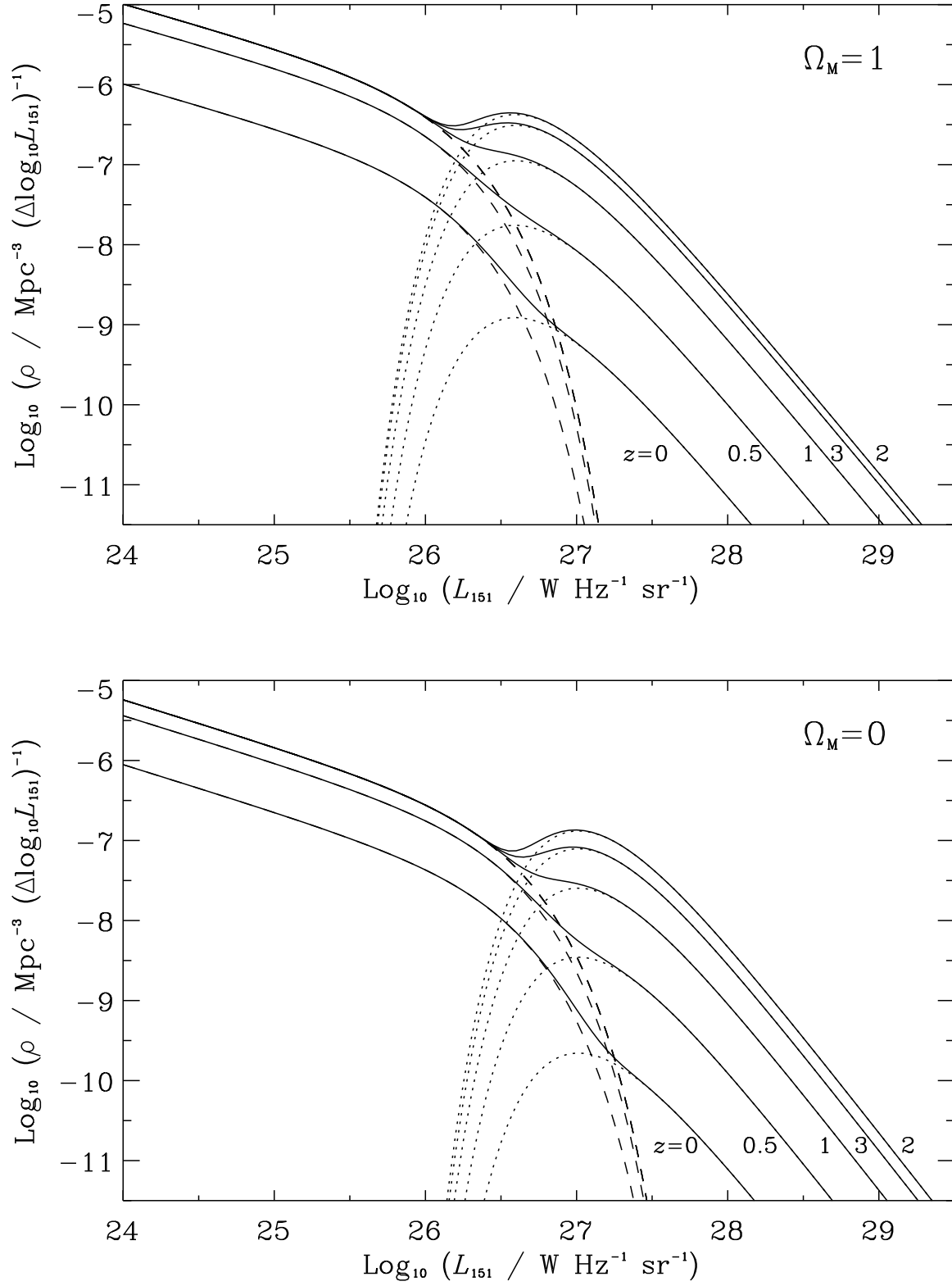


Figure 3. The radio luminosity function derived for model C for $\Omega_M = 1$ (top panel) and $\Omega_M = 0$ (bottom panel). Dashed lines show the low-luminosity population at $z = 0$, $z = 0.5$ and $z \gtrsim 0.7$ (bottom to top). The dotted lines are the high-luminosity RLF at $z = 0, 0.5, 1, 3$ and 2 (bottom to top). Solid lines show the sum of both components.

Model	Ω_M	$\log(\rho_{10})$	α_1	$\log(L_{1*})$	z_{10}	k_1	$\log(\rho_{h0})$	α_h	$\log(L_{h*})$	z_{h0}	z_{h1}	z_{h2}
A	1	-7.153	0.542	26.12	0.720	4.56	-6.169	2.30	27.01	2.25	0.673	-
B	1	-7.150	0.542	26.14	0.646	4.10	-6.260	2.31	26.98	1.81	0.523	-
C	1	-7.120	0.539	26.10	0.706	4.30	-6.196	2.27	26.95	1.91	0.559	1.378
A	0	-7.503	0.584	26.46	0.710	3.60	-6.740	2.42	27.42	2.23	0.642	-
B	0	-7.484	0.581	26.47	0.580	3.11	-6.816	2.40	27.36	1.77	0.483	-
C	0	-7.523	0.586	26.48	0.710	3.48	-6.757	2.42	27.39	2.03	0.568	0.956

Errors for model C ($\Omega_M = 1$): $\log(\rho_{10})$; $-0.11, +0.10$, α_1 ; $-0.02, +0.02$, $\log(L_{1*})$; $-0.09, +0.08$, z_{10} ; $-0.10, +0.10$, k_1 ; $-0.55, +0.57$, $\log(\rho_{h0})$; $-0.11, +0.09$, α_h ; $-0.11, +0.12$, $\log(L_{h*})$; $-0.10, +0.11$, z_{h0} ; $-0.16, +0.16$, z_{h1} ; $-0.05, +0.05$, z_{h2} ; $-0.28, +0.52$.

Table 1. Best-fit parameters for RLF models A, B and C, as described in Section 3.2. The top three rows refer to $\Omega_M = 1$ and the bottom three rows $\Omega_M = 0$.

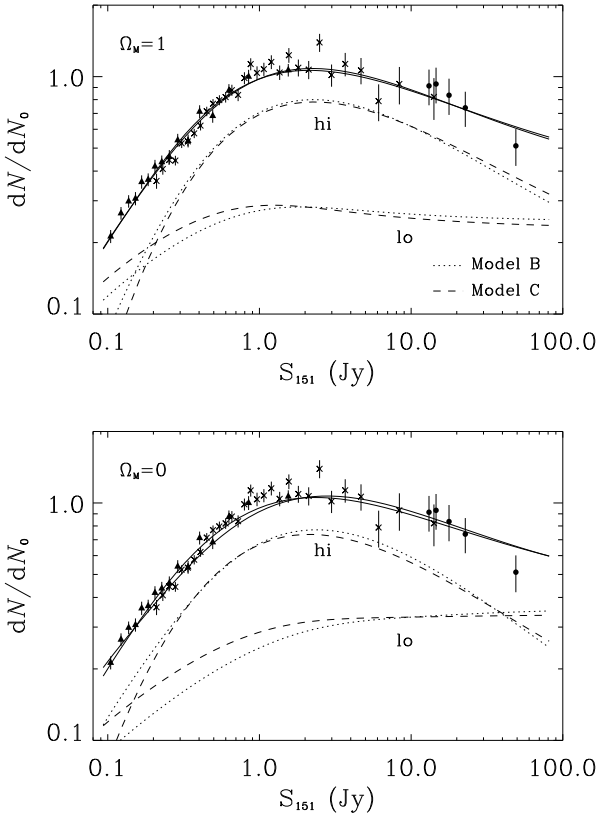


Figure 4. The 151 MHz source counts data (as in Fig. 2) with model-B (short-dash) and model-C (long-dash) fits for $\Omega_M = 1$ (top) and $\Omega_M = 0$ (bottom). The contributions to the source counts from the low-luminosity and the high-luminosity populations are shown separately (and marked ‘hi’ and ‘lo’). The solid lines show the total source counts from both models.

of the models for the two cosmologies considered. In both cosmologies the KS test shows that models B and C are marginally favoured over model A – the symmetric decline model. The extra parameter in model C (z_{h2} – the slope of the decline in number density at high-redshift) enables the strength of any high- z decline to be fitted directly. The fact that the best-fitting values of z_{h2} are greater than those of z_{h1} but less than infinity indicates a moderate high- z decline

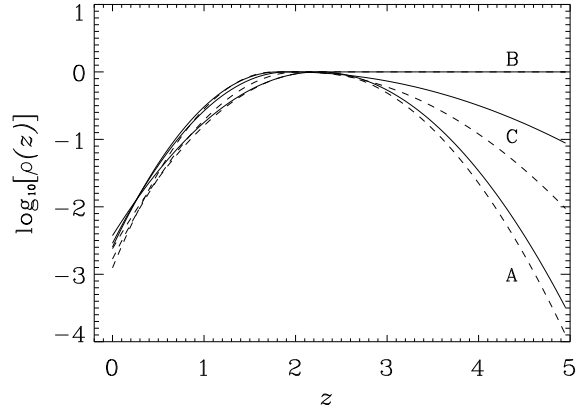


Figure 5. The best-fit redshift dependence of the high-luminosity part of the RLF for the 3 models considered here ($\Omega_M = 1$ – solid lines, $\Omega_M = 0$ – dashed lines). Note that the curves for model B in the two cosmologies are the same at high-redshift, so the dashed curve is obscured by the solid curve. All are normalised such that $\log_{10}(\rho) = 0$ at the peak redshift.

fits the data best (see Fig. 5). We conclude, however, that we cannot rule out with any level of confidence a constant space density up to $z \sim 5$.

3.4 Simulated data

Simulations of the $L_{151} - z$ plane for the three models are shown in Figure 6 along with the actual $L_{151} - z$ data for the complete samples (for $\Omega_M = 1$). Statements made in this section concerning comparison of real and simulated data apply also to an $\Omega_M = 0$ cosmology. The first thing to notice is that all the models reproduce the $L_{151} - z$ data reasonably well. Sources with emission line luminosities $\log_{10}(L_{[\text{OII}]} / W) \geq 35.1$ (see Willott et al. 1999, 2000 for discussion of this adopted value) are shown as filled symbols whereas those with lower luminosities are open. Note that because the radio galaxies in the combined sample span a large range of redshift, Balmer lines are often not observed and a classification scheme such as that adopted by Laing et al. (1994) to distinguish between low- and high-ionisation sources cannot be used. Therefore we make a distinction be-

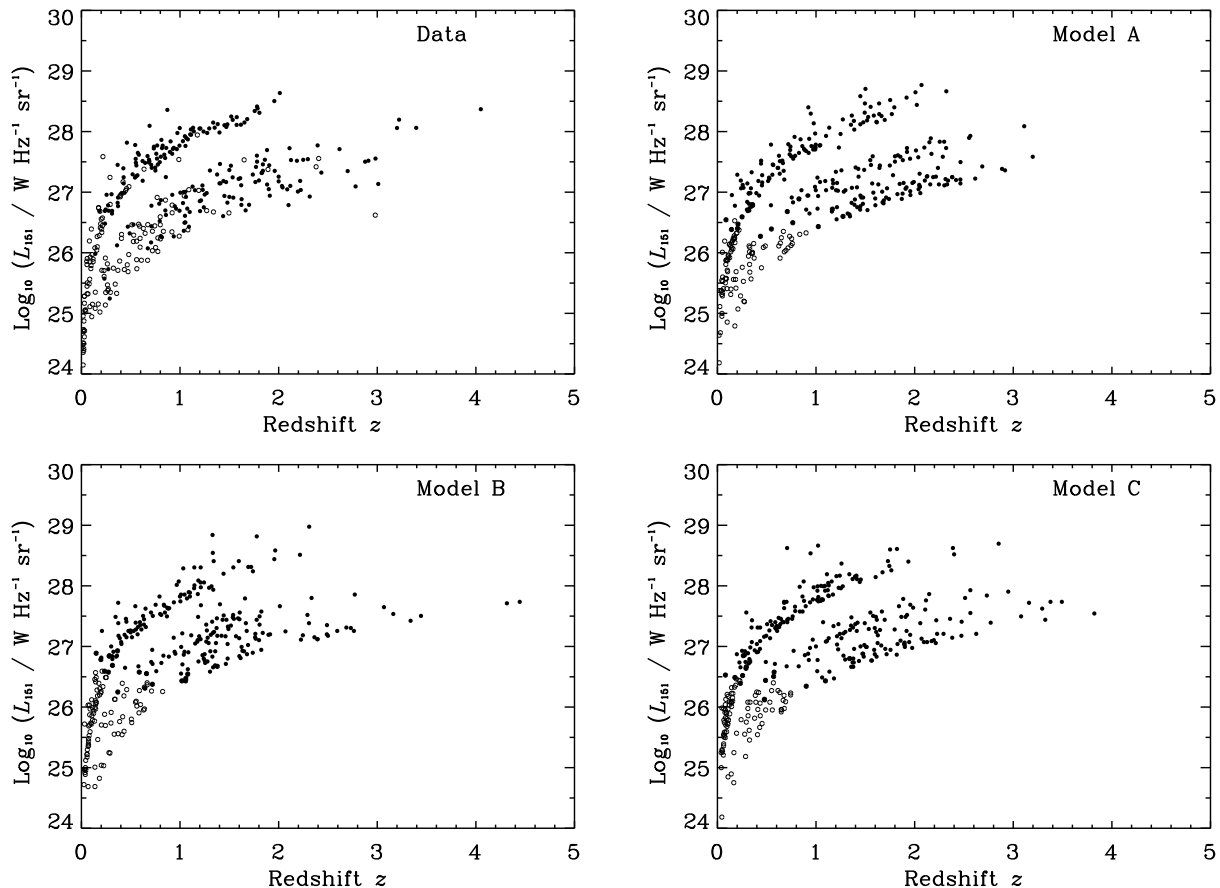


Figure 6. The top-left panel shows the $L_{151} - z$ plane for the 3CRR, 6CE and 7CRS complete samples. Objects in the samples with emission line luminosities $\log_{10}(L_{[\text{OII}]} / W) \geq 35.1$ are shown as filled symbols whilst those at lower luminosities are open. The other three panels show simulations of the $L_{151} - z$ plane for samples with the same flux-limits and sky areas as the complete samples. These simulations were generated using the best-fit RLF models A, B and C ($\Omega_M = 1$). Objects drawn from the low-luminosity population are shown as open circles and those from the high-luminosity population are open.

tween the two populations simply on the basis of emission line luminosity.

For the model simulations, the high and low luminosity populations are similarly separated into filled and open symbols. The transition between populations at $\log_{10}(L_{151} / W \text{ Hz}^{-1} \text{ sr}^{-1}) \approx 26.5$ is well-reproduced by the models indicating that the two populations can approximately be separated according to the strength of their narrow emission lines. As seen in Willott et al. (1999), this quantity is likely to be closely related to the accretion rate of the source. The scatter in the emission line–radio correlation is not taken account of in the RLF models, which explains why the filled and open symbols overlap in the real data, but do not for the simulations. This scatter is due to effects such as the range of radio source ages and environments which give different radio luminosities for a given jet power (see Willott et al. 1999; Blundell et al. 1999).

At high-redshifts ($z \approx 3$) the very few numbers of objects in the samples means that small number statistics become important. For a comparison with simulated data, the situation is even worse because both the data and the simulations have independent Poisson errors. Therefore, the simulations shown in this section should not be used to dis-

tinguish between best-fitting models (a direct integration of the RLF over redshift is preferable, see Sec. 3.5), but these simulations could give an indication of a poor fit. In any case, the simulations look very similar, even at $z \approx 3$, for all the three models tested.

3.5 Redshift distributions

We now consider the redshift distributions for the 3CRR, 6CE and 7CRS complete samples. As these are obtained by integrating the RLF, the only source of small number statistics come from the data they are compared with. Figure 7 shows histograms of the number of sources per bin of width $\delta z = 0.25$ for the 3CRR, 6CE and 7CRS samples separated into two populations depending upon emission line luminosities as before. For $\Omega_M = 0$, the high/low luminosity divide is at $\log_{10}(L_{[\text{OII}]} / W) = 35.4$. Also plotted are the model C RLF predictions for each population for the three samples.

For the 3CRR sample, the model fits very well, the main exception being the low luminosity objects at $z > 0.3$, where there are several more sources observed than predicted. This was also seen in the simulations and attributed to scatter in the emission line–radio correlation. With only 58 sources in

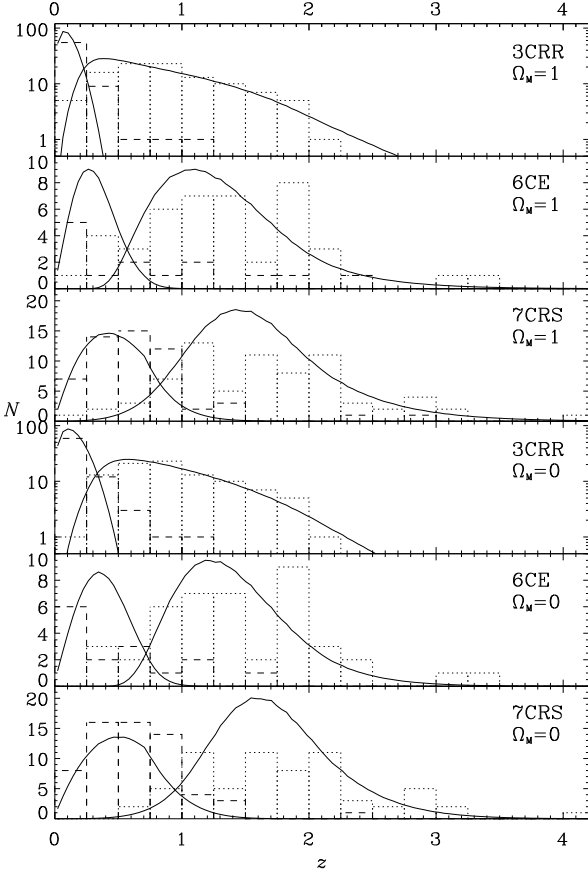


Figure 7. The histograms show the number of sources in the 3CRR, 6CE and 7CRS complete samples binned in redshift with bin width $\delta z = 0.25$ for $\Omega_M = 1$ and $\Omega_M = 0$. There are separate histograms for the low (dashed) and high (dotted) luminosity populations. The solid lines show the model C predictions for the number-redshift distribution for each population. Note that the 3CRR plot only has a log scale on the y-axis because of the high peak at low-redshift.

the 6CE sample, the effects of small number statistics are clear with an irregular observed distribution. However, in general the model redshift distribution is a fairly good approximation to the data. There is something of an excess of low-luminosity sources predicted at low-redshifts ($z < 0.5$), but this can be accounted for by the scatter, since there are several high-luminosity objects observed at these redshifts. For the 7CRS sample, again we find a fairly good fit. The main differences here are a small deficit predicted at $z \approx 0.5$ and an excess at $z \approx 1.5$. The redshift distributions at high-redshift ($z > 2$) will be discussed later in this section.

Figure 8 plots the cumulative redshift distributions of the two samples for all three models. The similarity of these three curves shows that the models all predict similar redshift distributions of sources. The one-dimensional KS test was used to test the difference between the observed and model redshift distributions. For the 3CRR sample the significances are 0.011 (0.03), 0.007 (0.03) and 0.007 (0.02) for models A, B and C, respectively ($\Omega_M = 0$ values in brackets). The values for the 6CE sample are 0.40 (0.32), 0.15 (0.10), 0.16 (0.18) and for the 7CRS sample 0.09 (0.002), 0.04 (0.0004) and 0.09 (0.001). The lowest values of KS sig-

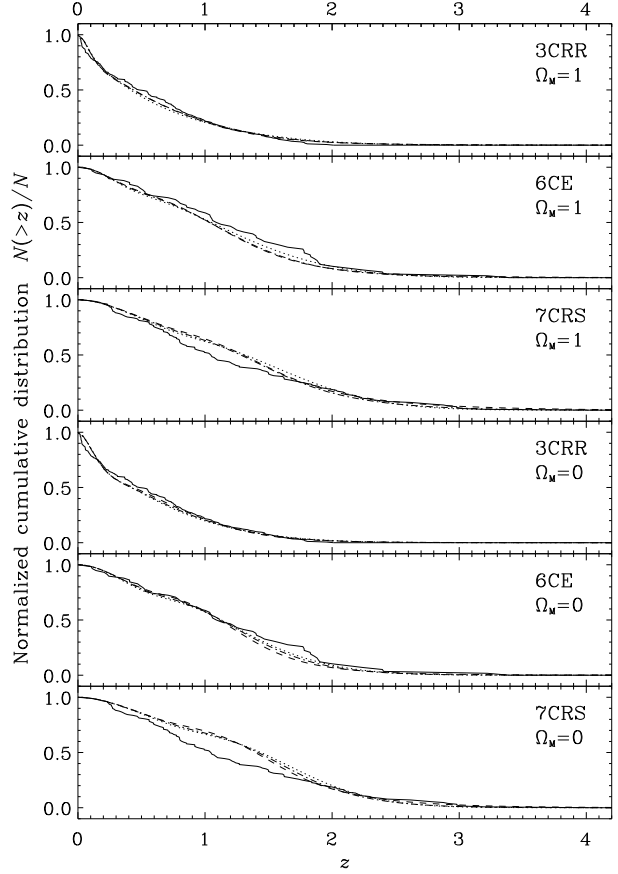


Figure 8. Normalised cumulative redshift distributions of sources in the 3CRR, 6CE and 7CRS complete samples. The solid curves are the cumulative redshift distributions in the samples predicted by the RLF of models A (dotted), B (dashed) and C (dot-dashed).

nificance are for the 7CRS redshift distribution for the case of $\Omega_M = 0$. It is fairly easy to speculate on the cause of this low probability: the model RLFs appear to be too high at $z \sim 1.5$ and $\log_{10} L_{151} \sim 26.5$ and too low at $z \sim 0.5$ and $\log_{10} L_{151} \sim 26$ ($\Omega_M = 1$, for $\Omega_M = 0$ these luminosities are $\log_{10} L_{151} \sim 26.9$ and 26.4). This is almost certainly a limitation of our modelling procedure since these luminosities lie close to the break luminosities L_{1*} and L_{h*} which bracket the range over which the two populations overlap. Away from these break luminosities the rates of exponential decline in luminosity of each population are fixed parameters in our model, and so their combination lacks the flexibility to fit perfectly all data within the overlap region. This situation could be improved by using additional free parameters, for example parameters controlling the rates of exponential decline, or by use of free-form fits (c.f. DP90).

To compare the numbers of high-redshift objects in the samples with the models, Fig. 9 plots the un-normalized cumulative redshift distributions at $z > 1.8$ on a logarithmic scale. For the 3CRR sample, model B (that with no decline in ρ at high-redshifts) predicts four sources at $z > 2$ ($\Omega_M = 1$; for $\Omega_M = 0$ the model predicts three sources) whereas there is only one observed. Using Poisson statistics the probability of observing one or less objects given a mean of four is 0.1. Therefore the observations are marginally in-

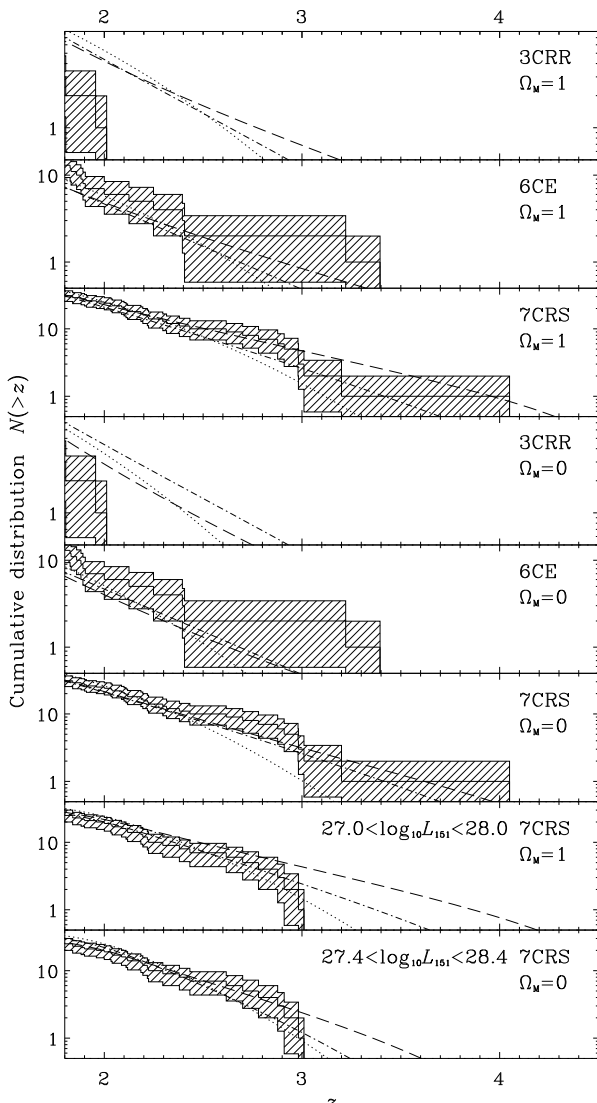


Figure 9. Cumulative redshift distributions at $z > 1.8$. Each panel shows the distributions predicted by each of models A, B & C as in Fig. 8. The data for each sample is shown as a solid line with the filled region the $\pm 1\sigma$ Poisson uncertainty. The top three panels refer to the 3CRR, 6CE and 7CRS samples, respectively, for $\Omega_M = 1$. The next three panels show the corresponding plots for $\Omega_M = 0$. The final two panels show the 7CRS cumulative redshift distributions including only sources with luminosities in the range $27.0 < \log_{10} L_{151} < 28.0$ ($\Omega_M = 1$) and $27.4 < \log_{10} L_{151} < 28.4$ ($\Omega_M = 0$).

compatible with the model. However, we note that the lack of $z > 2$ objects in the 3CRR sample could also be due to a steepening of the RLF at $\log_{10} L_{151} \sim 28.5$, due to a maximum radio luminosity of AGN, perhaps related to the maximum black hole mass in galaxies at these redshifts. This could be included in RLF models, but we do not do this in this paper, since there is little constraining data at such high luminosities and we wish to keep the numbers of free parameters in our models to a minimum. Note that the new equatorial sample of powerful radio sources defined by Best, Röttgering & Lehnert (1999) which has selection criteria producing a sample very similar to the 3CRR sample does indeed contain four sources at $z > 2$, so the lack of

such sources in the 3CRR sample may well be due to small number statistics. The evolution of the RLF for such high-luminosity sources is discussed in more detail in Jarvis et al. (2000).

Moving on to consider the 6CE and 7CRS redshift distributions (Fig. 9), we find that all three models are consistent with the high- z data to within 1σ uncertainties. There is no evidence here for a decline in the co-moving space density of radio sources at high-redshift.

The main benefit of the addition of the 7CRS complete sample to the existing 3CRR and 6CE samples, is that it enables the evolution in the luminosity band $27.0 < \log_{10} L_{151} < 28.0$ ($\Omega_M = 1$) to be determined over the wide redshift range $z \approx 0.3$ to $z \approx 3$ (see Fig. 1). DP90 found stronger evidence for a redshift cut-off in the steep-spectrum population by considering only the sources within a similar luminosity band (accounting for the difference in selection frequency). Therefore we now repeat our analysis using only the sources within this luminosity band (note that for $\Omega_M = 0$, the band chosen is that corresponding to equivalent source flux at $z = 2$, i.e. $27.4 < \log_{10} L_{151} < 28.4$). The bottom two panels of Fig. 9 repeat the 7CRS cumulative redshift distributions, but now including only those sources in these luminosity bands. For $\Omega_M = 1$, the no cut-off model B now appears inconsistent with the $z > 3$ data. The model predicts four sources at $z > 3$ whereas only one is observed. This gives the same probability as we found with the $z > 2$ 3CRR sources, i.e. a probability of 0.1 that the model and data are consistent. For the case of $\Omega_M = 0$, only two sources are predicted at $z > 3$ by the model, so this is certainly consistent with the observation of one source.

Thus we find very marginal evidence (90% confidence level) that the numbers of objects in the $27.0 < \log_{10} L_{151} < 28.0$ luminosity band falls slightly below the no cut-off model prediction. There is however, one systematic effect which might reduce even this significance. The expected numbers of high-redshift sources were calculated from the models assuming a spectral index between 151 MHz and $151 \times (1 + z)$ MHz of $\alpha = 0.8$. However, if high- z sources were systematically significantly steeper than $\alpha = 0.8$, then the expected number of high- z sources would be smaller. This is because a source of a given luminosity on the flux-limit with $\alpha = 0.8$, would clearly fall below the flux-limit if α were greater than this (see figure 1 in Blundell et al. 1999).

Our studies of complete samples (Blundell et al. 1999) do not reveal any intrinsic correlation between redshift and α evaluated at 151 MHz (α_{151}), however the correlation between luminosity and α_{151} will mean that any high-redshift sources (which must be high luminosity) will tend to have steeper spectral indices. The consequences of this effect are discussed in detail in Section 3 of Jarvis & Rawlings (2000) and we defer interested readers to that paper. Recalculation assuming $\alpha = 1.0$ at high-redshifts for model B gives an expectation of only two sources at $z > 3$, thereby removing any discrepancy between this model and the data. Finally, we note that the chosen luminosity band of $27.0 < \log_{10} L_{151} < 28.0$ excludes the four highest redshift objects in the combined sample (see Fig. 1) which have luminosities just above this limit. Extending the luminosity range considered to $27.0 < \log_{10} L_{151} < 28.5$ would give a similar result to those found for the entire samples.

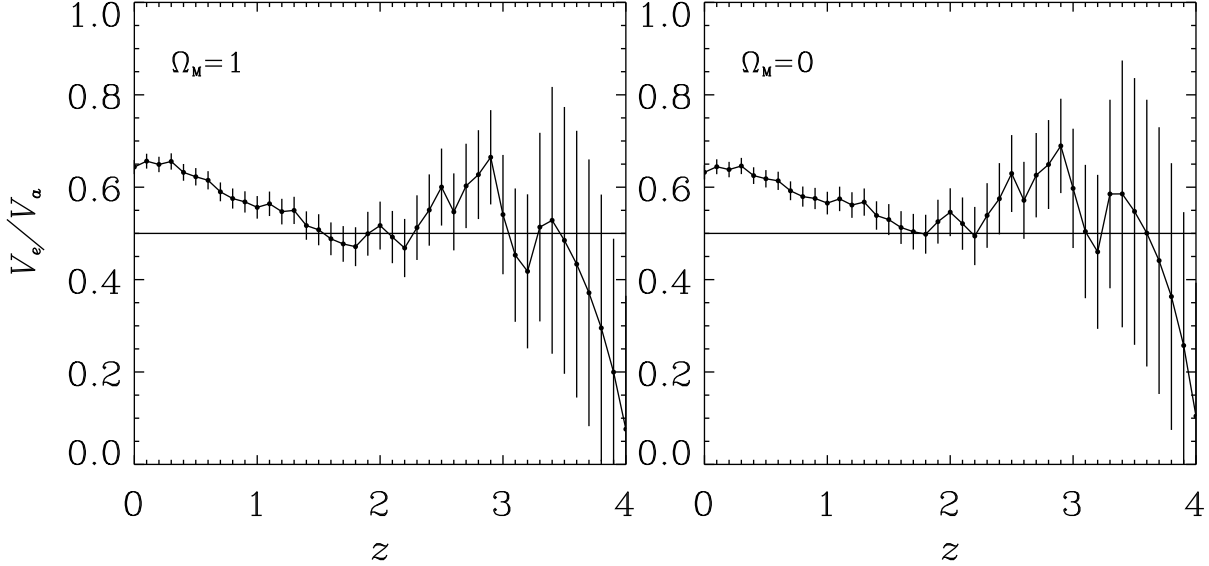


Figure 10. Banded V/V_{\max} test for the 356 sources in the 3CRR/6CE/7CRS complete samples. The left panel is for $\Omega_M = 1$ and the right panel for $\Omega_M = 0$. The error bars are equivalent to 1σ . There are no significant differences between the form of the V/V_{\max} tests for the two cosmologies.

4 THE V/V_{\max} TEST

In this section the V/V_{\max} test is applied to the complete sample data. This test calculates the ratio of the volume V in the Universe enclosed by each source of redshift z to the maximum volume V_{\max} , corresponding to the maximum redshift z_{\max} a source of this luminosity would have if its flux-density lies above one or more of the survey flux-limits. If there is no cosmic evolution then sources would have values of V/V_{\max} randomly distributed between 0 and 1 (Rowan-Robinson 1968; Schmidt 1968). Hence by calculating the values of V/V_{\max} for all the sources in a sample and averaging, one can determine the mean evolution of the sample. A value of $\langle V/V_{\max} \rangle$ greater than 0.5 corresponds to positive redshift evolution and less than 0.5 indicates negative evolution. The distribution of $\langle V/V_{\max} \rangle$ expected in the case of no evolution is, for a large sample size N , a Gaussian centred on 0.5 with $\sigma = (12N)^{-1/2}$.

Avni & Bahcall (1980) devised a method for combining samples with various flux-limits and sky areas for the application of a generalised V/V_{\max} test. This version combines several samples such that they can be treated as a single sample with a variable sky area depending upon the flux-limit. The new test variables are the volume enclosed by sources V_e and the volume available in the new sample V_a . Note also that the fact that the 6CE complete sample has an upper as well as a lower flux-limit means that the volume available for a source in the 6CE sample is given by $V_a = V_{\max} - V_{\min}$. To calculate values of V_a one must make some assumption about the shapes of the radio spectra to determine values of z_{\max} . For this test it is assumed that radio spectra are not significantly curved over the region of interest, and spectral indices at a rest-frame frequency of 151 MHz are used.

The known strong positive evolution from $z = 0$ to $z \approx 2$ would completely mask any change in the evolution

at higher redshifts in the standard V/V_{\max} test. Therefore a banded version of the test is used here (e.g. Osmer & Smith 1980). This modification calculates the mean V_e/V_a restricting the analysis to $z > z_0$ at several different values of z_0 . Hence all the evolution below z_0 is masked out of the analysis. The statistic is now

$$\frac{V_e - V_0}{V_a - V_0}, \quad (15)$$

where V_0 is the volume enclosed at redshift z_0 .

Fig. 10 shows this banded V/V_{\max} test for the complete samples. In the banded test, the adjacent points are not statistically independent and the error bars are much larger than the typical dispersion of points. Note that at low-redshifts ($z < 1.5$) the strong positive evolution of the radio source population is clearly seen with the values of V_e/V_a significantly above the 0.5 no-evolution line. At $z = 1.5$ the values approach the 0.5 line where they remain (within the errors) out to the redshift limit of this sample ($z = 4.0$). The positive bump at $z \approx 2.8$ is marginally significant, but at this point there are very few sources left in the sample, so no firm conclusions can be drawn from this. Thus there is no evidence from the V/V_{\max} test for a high- z decline (or increase) in the comoving space density of radio sources.

The V/V_{\max} test can also be used to study the evolution of the low- and high-luminosity populations separately. The complete samples were separated into two groups, depending upon their emission line luminosities as described in Sec. 3.4. These groups are supposed to signify the division between objects in the low- and high-luminosity populations in the RLF. The banded V/V_{\max} test was performed for each group and the results shown in Fig. 11. Both populations undergo positive evolution at low-redshift ($z < 0.5$) with the evolution stronger (and at a higher statistical significance) for the high-luminosity sources. At $z > 1$ most sources in the complete samples belong to the high-luminosity popu-

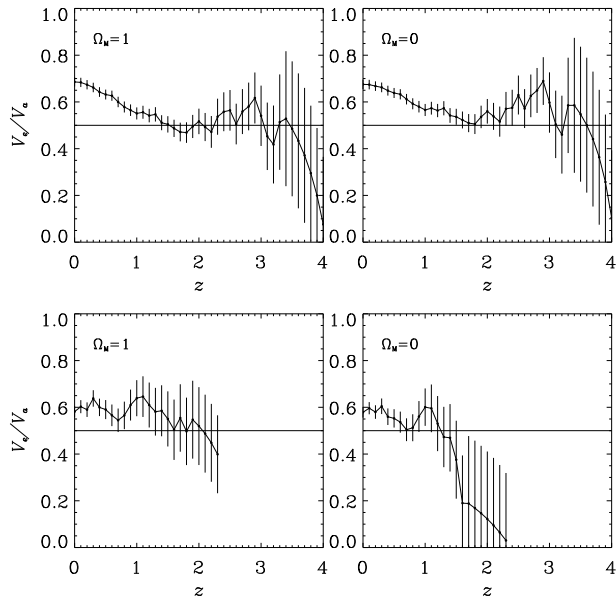


Figure 11. Banded V/V_{\max} test for the high- (top panels) and low- (bottom panels) luminosity populations separately. The left panels are $\Omega_M = 1$ and the right panels $\Omega_M = 0$.

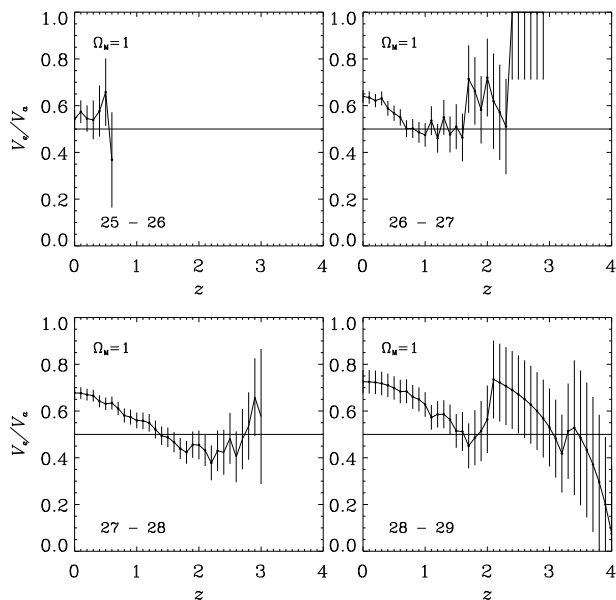


Figure 12. Banded V/V_{\max} test for the complete samples separated into different luminosity ranges. The ranges in $\log_{10} L_{151}$ included in each panel are labelled in the bottom-left corners ($\Omega_M = 1$ only is shown here).

lation, so its V/V_{\max} values are essentially the same as those in Fig. 10 for the whole dataset. There are hints of continuing positive evolution in the regime $0.5 < z < 1$ for the low-luminosity sources (this is more apparent for $\Omega_M = 1$ than $\Omega_M = 0$). This evolution of the low-luminosity population is consistent with that derived in the model RLFs, where the positive evolution ceases at $z \approx 0.7$.

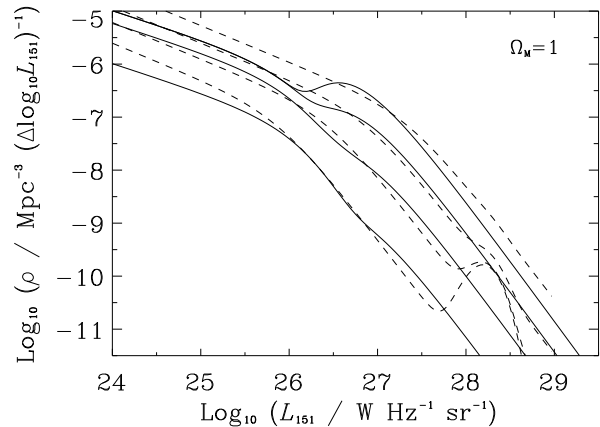


Figure 13. The evolving radio luminosity function of our model C (solid lines) plotted along with the PLE model of DP90 (dashed lines). The curves correspond to $z = 0, 0.5, 1, 2$ (bottom to top). The DP90 model has been transformed to 151 MHz by assuming all sources have spectral indices of 0.8.

In Fig. 12 we show the results of separating the sample into luminosity bands and repeating the V/V_{\max} test. The $0 < z < 1$ evolution appears to depend strongly on luminosity. The luminosity separation does not provide any evidence for negative evolution at high-redshifts (i.e. a redshift cut-off) in either of the two high-luminosity bands. Therefore we conclude from this Section that the V/V_{\max} test shows positive evolution at $z < 2$ which depends strongly on luminosity, but is inconclusive at higher redshifts.

5 COMPARISON WITH PREVIOUS WORK

5.1 Comparison with DP90

In Fig. 13, our model-C RLF is plotted with the steep-spectrum PLE model of DP90 at various redshifts ($\Omega_M = 1$ only). The DP90 LDE model which incorporates negative luminosity evolution at high-redshift is not shown here, since it is almost identical to the PLE model in the redshift range $0.5 < z < 3$ (which is to be expected as these regimes are constrained by data). To account for the fact that DP90 evaluated the RLF at high-frequency (2.7 GHz), their luminosity scale has been transformed to 151 MHz assuming a global spectral index of 0.8. The kinks in the DP90 model at $\log_{10}(L_{151}/\text{W Hz}^{-1} \text{sr}^{-1}) \approx 28.2$ are due to the use of a seven term power-law expansion for the non-evolving low-luminosity RLF component: there are no such powerful sources at low-redshift in their samples (or indeed in the 3CRR sample) and hence no constraint from the data, so this feature is a numerical artefact. As described in Sec. 3.5 our modelling procedure is also imperfect: the bumps in our estimations of the RLF around the breaks in the high- and low-luminosity populations may be artefacts of the restricted number of free parameters in our models.

In general, the DP90 PLE model and model C agree reasonably well. At low luminosities the PLE model has a steeper slope of 0.69 than the slope of model C (0.54). Again, this slope is only well constrained at low-redshifts and the cause of a differing slope is probably due to the use here

of a more recent determination of the local radio luminosity function. The break luminosity appears at exactly the same value for the two models. Note how our use of two populations with differential evolution mimics the evolution of the break luminosity in the PLE case. Since we know that radio sources are short-lived with respect to the Hubble Time, pure luminosity evolution has no physical meaning and there is clearly not one population of radio sources which fades over cosmic time. In contrast, the two population model has some physical meaning and mimics PLE by having only *density* evolution for both populations.

The high-luminosity power-law slopes for the DP90 PLE model and our model C are very similar. However, at $z = 2$ there is a clear excess of high-luminosity ($\log_{10} L_{151} > 27.5$) sources in the DP90 model. At $\log_{10} L_{151} = 28$ the DP90 RLF is a factor of 2.1 higher than that of our model C. At $z = 3$ and $\log_{10} L_{151} = 28$ this factor has increased to 2.4. The effect of this is shown by a comparison of the expected high-redshift sources in the 6CE sample for RLF models with no redshift cut-off in Dunlop (1998) and in this paper (Fig. 9). The plot by Dunlop shows a predicted excess at $z > 2$ over the number observed and this excess continues beyond the last data point at $z \approx 3.4$. Dunlop takes this as further evidence for the redshift cut-off. However, in Fig. 9 (second panel from top) we see that the 6CE redshift distribution is consistent with our model B at all redshifts. How can these two models, both of which claim to be no cut-off models, have such different predictions for the expected numbers of high-redshift sources? The answer is that all no cut-off models simply take the RLF at its peak at $z \approx 2$ and ‘freeze’ the shape and normalization up to high-redshifts (at least to $z \sim 5$). Therefore the DP90 models naturally predict more of these luminous sources at high redshifts because they have more of them at $z \approx 2$.

The next question is why do DP90 find a higher density of powerful sources at $2 \lesssim z \lesssim 3$ than found by our study? The answer is probably due to the fact that a very high fraction of the most distant sources in DP90 did not have reliable redshifts: inspection of fig. 9 of DP90 shows that only a quarter of their $z > 2$ steep-spectrum PSR sources had spectroscopic redshifts with the remainder estimated from the $K - z$ diagram. Dunlop (1998) reports that further spectroscopy has shown the redshifts in DP90 to be typically over-estimated (most likely due to the positive correlation between radio luminosity and K -band luminosity observed by Eales et al. 1997). If these sources are actually at systematically lower redshifts then this explains why DP90 observe an excess of $z > 2$ sources. Extrapolating this high source density up to $z = 5$ then predicts many sources in no cut-off models. Note that because few of their redshift estimates were actually in the region of supposed decline (at $z > 3$) the redshift over-estimation has the opposite effect to the naive expectation that this new information strengthens claims for the redshift cut-off. Thus we have an explanation as to why DP90 find stronger evidence for a steep-spectrum redshift cut-off than we find with the 3CRR, 6CE and 7CRS datasets (having virtually complete spectroscopic redshifts).

DP90 argued that their V/V_{\max} test on the steep-spectrum population showed clear evidence for a redshift cut-off beyond $z = 2$. However we do not find a similar behaviour in our low-frequency selected samples, with apparently no evolution between $z = 2$ and $z = 4$. Inspection

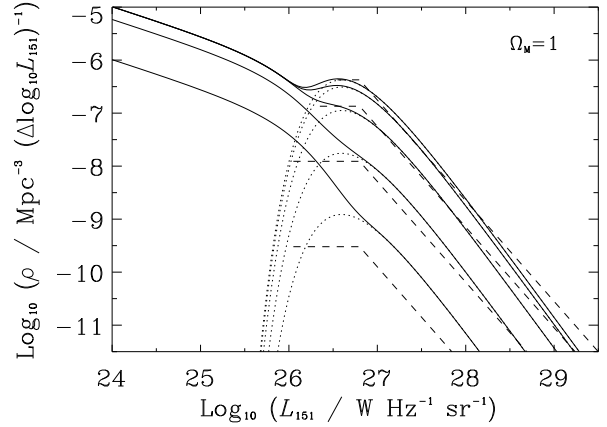


Figure 14. The evolving radio luminosity function of model C (solid lines) plotted along with the quasar RLF model C from W98 (dashed lines). The quasar RLF has been multiplied by a factor of 2.5 to account for the fraction of luminous quasars compared to radio galaxies in low-frequency selected samples above the critical luminosity $\log_{10} L_{151} \approx 26.5$ (Willott et al. 2000). Also plotted as dotted lines is the high-luminosity part of the model-C RLF. The curves correspond to $z = 0, 0.5, 1, 3, 2$ (bottom to top).

of figs. 12 and 13 of DP90 show that their evidence of negative density evolution at $z \gtrsim 2$ is highly tentative: their data are only about 1σ away from the null-hypothesis of no evolution. The banded V/V_{\max} test suffers significantly from large statistical errors when only a few sources are left in the samples at the highest redshifts, and this tends to limit its usefulness in practice. Combined with the uncertainty in the DP90 redshift estimates, it is difficult to see clear evidence for a redshift cut-off in their V/V_{\max} tests.

5.2 Comparison with the radio-loud quasar RLF

In line with unified schemes (e.g. Antonucci 1993), the high-luminosity part of the RLF derived here consists of radio galaxies and quasars which are identical except for the angle our line-of-sight makes with the jet axis. In Willott et al. (2000) we showed that the fraction of quasars in the high luminosity population is 0.4. Therefore one would expect a very similar RLF to that of the quasars in W98, with an increase in number density of ≈ 2.5 . Fig. 14 plots the RLF derived for all radio sources in this paper and the quasar RLF from W98 multiplied by a factor of 2.5. At high-redshifts the two RLFs appear very similar (there are very few low-redshift/luminosity quasars in the complete samples – see Willott et al. 2000 for a discussion of this). The high-luminosity power-law slope for model C is 2.3, compared with 1.9 for the quasar RLF. The peak for the high-luminosity Schechter function is at approximately the same luminosity ($\log_{10}(L_{151}) \approx 26.6$) as the break required by the source counts for the quasar RLF. The quasar RLF of W98 had a flat slope below this break, whereas the models of this paper have very rapid declines with decreasing luminosity. If the models described here are correct, then the quasar RLF should also have this Schechter function form. A survey at fainter flux-limits would probe the break region at high-

redshift and hopefully constrain the number of quasars (or BLRGs) at lower radio luminosities. A sample of quasars with a flux-limit of $S_{151} \geq 0.1$ Jy has already been defined by Riley et al. (1999), however incompleteness arising from the bright optical limit of this sample (as discussed by W98) will complicate attempts to make quantitative estimates of the shape of the RLF at and below the break luminosity.

6 DISCUSSION

Using low-frequency selected radio samples with virtually complete redshift information, we have investigated the form of the radio luminosity function (RLF) and its evolution. Our results are generally in good agreement with previous work by DP90 (Fig.13) and W98 (Fig. 14), and most discrepancies can be explained by limitations of the modelling methods forced on this and previous studies by the sparse sampling of the $L - z$ plane afforded by available redshift surveys of radio sources. For the reasons outlined in Sec. 1, most notably our virtually complete spectroscopic redshifts, we believe our estimates of the steep-spectrum RLF to be the most accurate yet obtained.

We find that a simple dual-population model for the RLF fits the data well, requiring differential density evolution (with z) for the two populations. This behaviour mimics the effects of a pure luminosity evolution (PLE) model but with a more plausible physical basis. The low-luminosity population can be associated with radio galaxies with weak emission lines, and includes sources with both FRI and FRII radio structures. The comoving space density ρ of the low-luminosity population rises by about one dex between $z \sim 0$ and $z \sim 1$ but cannot yet be meaningfully constrained at higher redshifts. The high-luminosity population can be associated with radio galaxies and quasars with strong emission lines, and consists almost exclusively of sources with FRII radio structure. The comoving space density ρ of this population rises by nearly three dex between $z \sim 0$ and $z \sim 2$ but cannot yet be meaningfully constrained at higher redshifts.

Our results on the RLF mirror the situation seen in X-ray and optically-selected samples of AGN. Low luminosity objects exhibit a gradual [$\propto (1+z)^{-3.5}$ from $z \sim 0$ to $z \sim 1$] rise in ρ with z which matches the rise seen in the rate of global star formation (e.g. Boyle & Terlevich 1998; Franceschini et al. 1999), and also the rise in the galaxy merger rate (e.g. Le Fevre et al. 2000). The ρ of high-luminosity objects rises much more dramatically [$\propto (1+z)^{-5.5}$ from $z \sim 0$ to $z \sim 2$]. The similarities between the cosmic evolution of radio sources and these different types of objects have also been pointed out by Wall (1998) and Dunlop (1998).

We have re-investigated the question of whether there is direct evidence for a high-redshift decline in the comoving space density ρ of steep-spectrum radio sources. Applying the V/V_{\max} test to the 3C/6CE/7CRS dataset provides no evidence for any such decline, which is a different result from that obtained by DP90. A fundamental limitation is that both our complete samples and those previously studied by DP90 include only a few sources with $z > 2.5$ (e.g. just 12 in 3C/6CE/7CRS), so small number statistics are a huge problem in assessing the evidence for or against a redshift cut-off. This is considered in detail in Jarvis et al. (2000).

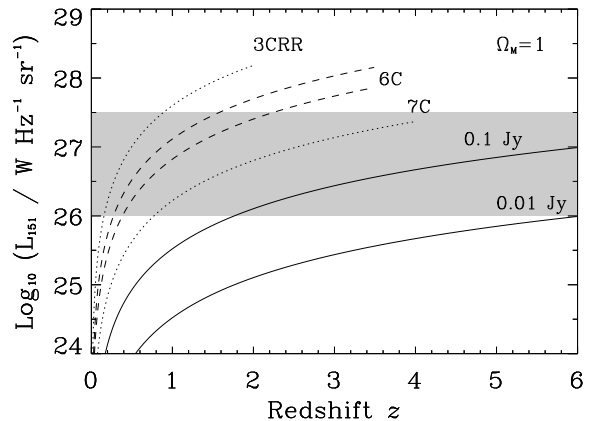


Figure 15. The flux-limits on the radio luminosity – redshift plane for low-frequency selected samples. The shaded band shows the luminosity range near the break in the RLF which contains 70 % of the luminosity density at high-redshifts.

What would be the best way of clearing up this uncertainty regarding the redshift cut-off? Larger samples are clearly needed, but in the case of the bright samples like 3CRR, there is insufficient observable Universe to improve much on the data already available. Significant progress on fainter radio samples is however achievable. The choice of the flux-density level at which to concentrate efforts for the next large redshift survey is clearly crucial. We believe that the vital factor is being able to efficiently probe objects at or just above the break in the high-luminosity RLF at high-redshift. The reason for this is that integration of $\rho \times L_{151}$ over the RLFs plotted in Fig. 3 shows that about 70% of the luminosity density of the radio population at $z \sim 2 - 3$ lies in the narrow luminosity range $26 \leq \log_{10} L_{151} \leq 27.5$. A future large redshift survey should be targeted at probing this population, which is seen only to $z \sim 1$ in the 7CRS. Fig. 15 shows flux-limits in the $L_{151} - z$ plane for various samples with this luminosity range shaded. The plot illustrates that $S_{151} \sim 0.1$ Jy is therefore the natural choice for a new large redshift survey. Fainter surveys would be less useful as a probe of the total luminosity density at high-redshift: inspection of Fig. 15 shows that they would become completely dominated by the low-luminosity population,

To investigate the likely content of a $S_{151} > 0.1$ Jy redshift survey, we have used models A, B and C RLFs to predict redshift distributions for a hypothetical 1000-source survey (Fig. 16). Note that all models assume that the evolution of the low-luminosity population freezes at $z \sim 1$. The first thing to notice is that the low-luminosity population dominates the total number of predicted sources in the case of $\Omega_M = 1$, whereas in the $\Omega_M = 0$ case the two populations become approximately equal. This same result can be seen in the source counts plots of Fig. 4, and arises because the low-luminosity RLF is currently constrained only at low-redshift, and the ratio of high- to low-redshift available volume is much larger in a low- Ω_M Universe. Thus, although a large fraction of the sources will be at $z < 1$, we predict that in a low- Ω_M Universe in which evolution of the low-luminosity population freezes at $z \sim 1$, of order 50 % of the sources will be in the high-luminosity popula-

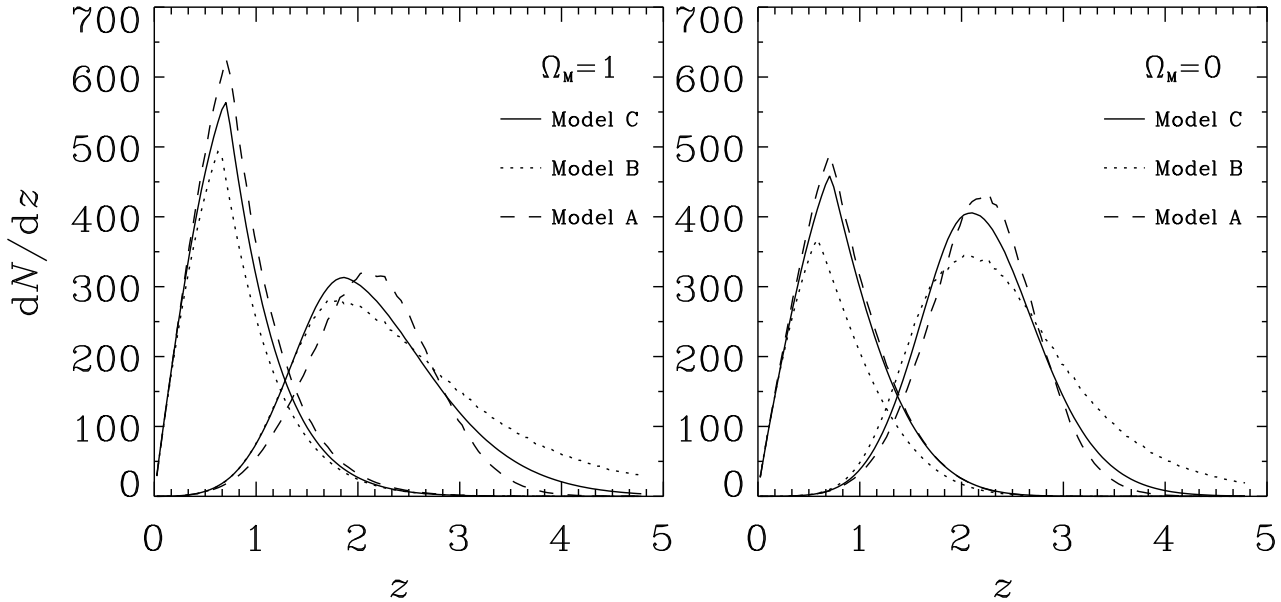


Figure 16. The predicted redshift distribution of a sample selected at a radio flux-limit of $S_{151} \geq 0.1$ Jy (five times lower than the 7CRS) for $\Omega_M = 1$ (left) and $\Omega_M = 0$ (right). The low and high luminosity populations are plotted separately, each for the three models A, B and C. The vertical axis is the number of sources per unit redshift. The plots are normalised such that the total number of sources in the sample equals 1000.

tion and lie at high-redshift, irrespective of the strength of the redshift cut-off. This should make determination of the evolution in the luminosity density a rather straightforward process. There should be no longer be a problem of small number statistics, at least at $z \sim 3$. Adopting model C, 7% (5%) of a hypothetical 1000-source redshift survey would lie at $z \geq 3$ for $\Omega_M = 1$ (or $\Omega_M = 0$), whereas the same model predicts 3% (2%) for a survey like the 7CRS.

The pronounced high-redshift tail in the case of ‘no-cut-off’ model B in Fig. 16 should be easily refutable with a 1000-source redshift survey at $S_{151} > 0.1$ Jy. For the symmetric-decline model A (and $\Omega_M = 1$) one would expect about 35 $z \geq 3$ sources in such a sample, whereas for model B we would expect 130. Indeed, Dunlop (1998) has already claimed to have ruled out the no-cut-off case using indirect constraints on the redshift distribution of a LBDS (Leiden-Berkeley Deep Survey) sample flux-limited at $S_{1.4} \sim 2$ mJy, or $S_{151} \sim 10$ mJy. We note from Fig. 15 that such a sample will be overwhelmingly dominated by the low-luminosity population, and hence is too deep to provide optimal constraint on the evolution of the luminosity density of the RLF. Although, as we shall argue below, indirect evidence favours a gentle decline in ρ at high-redshift, Dunlop’s argument in favour of a redshift cut-off is not water-tight. It is currently predicated on an extrapolation between two samples, the PSR and the LBDS sample, neither of which is close to spectroscopic completeness, and which are separated by two orders of magnitude in flux-density; at high-redshift the PSR and LBDS sources lie on either side of the range in L_{151} which is key to delineating the evolution of the luminosity density of the radio source population with redshift.

An alternative approach to obtaining complete redshift information for large samples is to refine the sample selection criteria to exclude the large numbers of low-redshift sources. This is being attempted by several groups using spectral

index and/or linear size criteria (e.g. Bremer et al. 1998; Blundell et al. 1998; Rawlings et al. 1998; De Breuck et al. 2000). However, the numbers of high- z sources which are missed in these samples are uncertain, so they will always struggle to prove the existence of a redshift cut-off, although they can place a lower limit on the space density (Jarvis et al. 2000).

Another alternative approach is to study the evolution of flat-spectrum radio sources. Jarvis & Rawlings (2000) have recently critically re-evaluated evidence in this area (Peacock 1985; DP90; Shaver et al. 1996; Shaver et al. 1999) and concluded that constant- ρ models for the most luminous flat-spectrum sources can be ruled out at the $\sim 2\sigma$ level. They favour a decline in ρ for these objects by a factor ~ 3 between $z \sim 2.5$ and $z \sim 5$, i.e. behaviour intermediate between models B and C considered in this paper. However, they also point out that it is not yet clear how this decline should be interpreted in the context of the steep-spectrum population.

7 CONCLUSIONS

- We have used three low-frequency selected surveys with essentially complete spectroscopic redshift information, giving unprecedented coverage of the radio luminosity versus z plane, to derive the most accurate measurement of the steep-spectrum RLF yet made.

- We find that a simple dual-population model for the RLF fits the data well, requiring differential density evolution (with z) for the two populations.

- The low-luminosity population can be associated with radio galaxies with weak emission lines, and includes sources with both FRI and FRII radio structures; its comoving space density ρ rises by about one dex between $z \sim 0$ and $z \sim 1$ but cannot yet be meaningfully constrained at higher redshifts.

The high-luminosity population can be associated with radio galaxies and quasars with strong emission lines, and consists almost exclusively of sources with FR II radio structure; its ρ rises by nearly three dex between $z \sim 0$ and $z \sim 2$.

8 ACKNOWLEDGEMENTS

Thanks to Gary Hill, Julia Riley and David Rossitter for their important contributions to the 7C Redshift Survey. Thanks also to Matt Jarvis and Jasper Wall for interesting discussions. We thank the referee Jim Dunlop for a helpful referees report. We acknowledge the use of the UKIRT, the WHT and the NRAO VLA which have together made this project possible. The United Kingdom Infrared Telescope is operated by the Joint Astronomy Centre on behalf of the U.K. Particle Physics and Astronomy Research Council. The William Herschel Telescope is operated on the island of La Palma by the Isaac Newton Group in the Spanish Observatorio del Roque de los Muchachos of the Instituto de Astrofísica de Canarias. The Very Large Array is operated by The National Radio Astronomy Observatory which is a facility of the National Science Foundation operated under cooperative agreement by Associated Universities, Inc. This research has made use of the NASA/IPAC Extra-galactic Database, which is operated by the Jet Propulsion Laboratory, Caltech, under contract with the National Aeronautics and Space Administration. CJW thanks PPARC for support.

REFERENCES

Antonucci R.R.J., 1993, *ARAA*, 31, 473
 Avni Y., Bahcall J.N., 1980, *ApJ*, 235, 694
 Baum S.A., Heckman T.M., 1989, *ApJ*, 336, 702
 Best P.N., Röttgering H.J.A., Lehnert M.D., 1999, *MNRAS*, 310, 223
 Blundell K.M., Rawlings S., 1999, *Nature*, 399, 330
 Blundell K.M., Rawlings S., Eales S.A., Taylor G.B., Bradley A.D., 1998, *MNRAS*, 295, 265
 Blundell K.M., Rawlings S., Willott C.J., 1999, *AJ*, 117, 677
 Boyle B.J., Terlevich R.J., 1998, *MNRAS*, 293L, 49
 Boyle B.J., Shanks T., Peterson B.A., 1988, *MNRAS*, 235, 935
 Bremer M.N., Rengelink R., Saunders R., Röttgering H.J.A., Miley G.K., Snellen I.A.G., 1998, in *Observational Cosmology with the New Radio Surveys*, eds. M.N. Bremer et al., 165, Kluwer
 Cavaliere A., Padovani P., 1989, *ApJ*, 340, L5
 Condon J.J., 1984, *ApJ*, 284, 44
 Condon J.J., Cotton W.D., Greisen E.W., Yin Q.F., Perley R.A., Taylor G.B., Broderick J.J., 1998, *AJ*, 115, 1693
 Cotton W.D., Condon J.J., 1998, in *Observational Cosmology with the New Radio Surveys*, eds. M.N. Bremer et al., 45, Kluwer
 De Breuck C., van Breugel W., Röttgering H.J.A., Miley G., 2000, *A&AS*, 143, 303
 Dunlop J.S., 1998, in *Observational Cosmology with the New Radio Surveys*, eds. M.N. Bremer et al., 157, Kluwer
 Dunlop J.S., Peacock J.A., 1990, *MNRAS*, 247, 19 (DP90)
 Eales S.A., 1985, *MNRAS*, 217, 149
 Eales S.A., Rawlings S., Law-Green J.D.B., Cotter G., Lacy M., 1997, *MNRAS*, 291, 593
 Fanaroff B.L., Riley J.M., 1974, *MNRAS*, 167, 31P

Franceschini A., Hasinger G., Miyaji T., Malquori D., 1999, *MNRAS*, 310L, 5
 Gardner J.P., Sharples R.M., Frenk C.S., Carrasco B.E., 1997, *ApJ*, 480, L99
 Goldschmidt P., Miller L., 1998, *MNRAS*, 293, 107
 Hales S.E.G., Baldwin J.E., Warner P.J., 1988, *MNRAS*, 234, 919
 Hine R.G., Longair M.S., 1979, *MNRAS*, 188, 111
 Jackson C.A., Wall J.V., 1999, *MNRAS*, 304, 160
 Jarvis M.J., Rawlings S., 2000, *MNRAS*, in press, astro-ph/0006081
 Jarvis M.J., Rawlings S., Willott C.J., Blundell K.M., Eales S.A., Lacy M., 2000, *MNRAS*, submitted
 Kaiser, C.R., Alexander P., 1997, *MNRAS*, 286, 215
 Kochanek C.S., 1996, *ApJ*, 473, 595
 Lacy M., Rawlings S., Hill G.J., Bunker A.J., Ridgway S.E., Stern D., 1999a, *MNRAS*, 308, 1096
 Lacy M., Kaiser M.E., Hill G.J., Rawlings S., Leyshon G., 1999b, *MNRAS*, 308, 1087
 Lacy M., Bunker A.J., Ridgway S.E., 2000, *AJ*, 120, 68
 Laing R.A., Riley J.M., Longair M.S., 1983, *MNRAS*, 204, 151 (LRL)
 Laing R.A., Jenkins C.R., Wall J.V., Unger S.W., 1994, in *Proceedings of the Stromlo Centenary Symposium: Physics of Active Galactic Nuclei*, ed. G. Bicknell, 201, Springer-Verlag, Berlin
 Le Fèvre O., Abraham R., Lilly S.J., Ellis R.S., Brinchmann J., Schade D., Tresse L., Colless M., Crampton D., Glazebrook K., Hammer F., Broadhurst T., 2000, *MNRAS*, 311, 565
 Longair M.S., 1966, *MNRAS*, 133, 421
 Magliocchetti M., Maddox S.J., Lahav O., Wall J.V., 1998, *MNRAS*, 300, 257
 McGilchrist M.M., Baldwin J.E., Riley J.M., Titterton D.J., Waldram E.M., Warner P.J., 1990, *MNRAS*, 246, 110
 Miyaji T., Hasinger G., Schmidt M., 2000, *A&A*, 353, 25
 Nilson P., 1973, *Uppsala General Catalogue of Galaxies*, Uppsala Astronomical Observatory
 Osmer P.S., Smith M.G., 1980, *ApJS*, 42, 333
 Padovani P., Urry C.M., 1992, *ApJ*, 387, 449
 Page M.J., Carrera F.J., Hasinger G., Mason K.O., McMahon, R.G., Mittaz J.P.D., Barcons X., Carballo R., Gonzalez-Serrano I., Perez-Fournon I., 1996, *MNRAS*, 281, 576
 Peacock J.A., 1983, *MNRAS*, 202, 615
 Peacock J.A., 1985, *MNRAS*, 217, 601
 Rawlings S., Saunders R., 1991, *Nature*, 349, 138
 Rawlings S., Blundell K.M., Lacy M., Willott C.J., Eales S.A., 1998, in *Observational Cosmology with the New Radio Surveys*, eds. M.N. Bremer et al., 171, Kluwer
 Rawlings S., Eales S.A., Lacy M., 2000, *MNRAS*, in press
 Rees M.J., Setti G., 1968, *Nature*, 219, 127
 Riley J.M., 1989, *MNRAS*, 238, 1055
 Riley J.M., Rawlings S., McMahon R.G., Blundell K.M., Miller P., Lacy M., 1999, *MNRAS*, 307, 293
 Rixon G.T., Wall J.V., Benn C.R., 1991, *MNRAS*, 251, 243
 Rowan-Robinson M., 1968, *MNRAS*, 138, 445
 Saunders W., Rowan-Robinson M., Lawrence A., Efstathiou G., Kaiser N., Ellis R.S., Frenk C.S., 1990, *MNRAS*, 242, 318
 Schmidt M., 1968, *ApJ*, 151, 393
 Shaver P.A., Wall J.V., Kellermann K.I., Jackson C., Hawkins M.R.S., 1996, *Nature*, 384, 439
 Shaver P.A., Hook I.M., Jackson C., Wall J.V., Kellermann K.I., 1999, in *Highly Redshifted Radio Lines*, eds. C.L. Carilli et al., ASP Conf. Series Vol. 156, 163.
 Urry C.M., Padovani P., 1995, *PASP*, 107, 803
 Urry C.M., Padovani P., Stickel M., 1991, *ApJ*, 382, 501
 Wall J.V., 1983, in *The Origin and Evolution of Galaxies*, eds. B.J.T. Jones and J.E. Jones, 295, Reidel
 Wall J.V., 1998, in *Observational Cosmology with the New Radio Surveys*, eds. M.N. Bremer et al., 129, Kluwer

- Wall J.V., Pearson T.J., Longair M.S., 1980, MNRAS, 193, 683
Warren S.J., Hewett P.C., Osmer P.S., 1994, ApJ, 421, 412
Willott C.J., Rawlings S., Blundell K.M., Lacy M., 1998, MNRAS, 300, 625 (W98)
Willott C.J., Rawlings S., Blundell K.M., Lacy M., 1999, MNRAS, 309, 1017
Willott C.J., Rawlings S., Blundell K.M., Lacy M., 2000, MNRAS, 316, 449
Willott C.J., Rawlings S., Blundell K.M., 2000, MNRAS, in press
Windhorst R.A., Miley G.K., Owen F.N., Kron R.G., Koo D.C., 1985, ApJ, 289, 494